A

B

Sham   TAC   TAC+CADO

C

D

Figure 6. Improvement of heart function in vivo by CADO. A, Lung weight to body weight (LW/BW) ratio was attenuated by CADO or CPA. *$P<0.01$, **$P<0.0001$. Numbers of mice in every group and abbreviations are the same as in Figure 5B. B, Representative lungs of mice treated with sham, TAC, or TAC+CADO (bar=1 mm). C, LVFS. *$P<0.05$. The number of mice in sham, TAC, TAC+CADO, TAC+CADO+SPT, TAC+SPT, TAC+CPA, and TAC+CPA+DPCPX groups is 14, 22, 15, 7, 17, 6, and 6 respectively. D, LV dP/dt $_{max}$ was increased in CADO- or CAP-treated mice. *$P<0.05$, n=5 in every group. Values are mean±SEM. .

level to be able to act at the receptor level in pressure-overload state. Therefore, it would be of importance to clarify whether augmentation of endogenous adenosine is beneficial to cardiac hypertrophy.

In conclusion, the data in this study indicate that the activation of adenosine A_1 receptors attenuates both the cardiac hypertrophy and myocardial dysfunction mediated by combined mechanisms of antiadrenergic effect and upregulation of RGS-4.

Acknowledgments

References

1. Sadoshima J, Izumo S. Molecular characterization of angiotensin II–induced hypertrophy of cardiac myocytes and hyperplasia of cardiac fibroblasts: critical role of the AT_1 receptor subtype. Circ Res. 1993;73: 413–423.

2. Akers WS, Cross A, Speth R, Dwoskin LP, Cassis LA. Renin-angiotensin system and sympathetic nervous system in cardiac pressure-overload hypertrophy. Am J Physiol Heart Circ Physiol. 2000;279:H2797–H2806.

3. Dostal DE, Baker KM. Angiotensin and endothelin: messengers that couple ventricular stretch to the Na^+/H^+ exchanger and cardiac hypertrophy. Circ Res. 1998;83:870–873.

4. Schafer M, Ponicke K, Heinroth-Hoffmann I, Brodde OE, Piper HM, Schluter KD. β-Adrenoceptor stimulation attenuates the hypertrophic effect of α-adrenoceptor stimulation in adult rat ventricular cardiomyocytes. J Am Coll Cardiol. 2001;37:300–307.

5. Deng XF, Rokosh DG, Simpson PC. Autonomous and growth factor-induced hypertrophy in cultured neonatal mouse cardiac myocytes: comparison with rat. Circ Res. 2000;87:781–788.

6. Asakura M, Kitakaze M, Takashima S, Liao Y, Ishikura F, Yoshinaka T, Ohmoto H, Node K, Yoshino K, Ishiguro H, Asanuma H, Sanada S, Matsumura Y, Takeda H, Beppu S, Tada M, Hori M, Higashiyama S. Cardiac hypertrophy is inhibited by antagonism of ADAM12 processing of HB-EGF: metalloproteinase inhibitors as a new therapy. Nat Med. 2002;8:35–40.

7. Patel R, Lim DS, Reddy D, Nagueh SF, Lutucuta S, Sole MJ, Zoghbi WA, Quinones MA, Roberts R, Marian AJ. Variants of trophic factors and expression of cardiac hypertrophy in patients with hypertrophic cardiomyopathy. J Mol Cell Cardiol. 2000;32:2369–2377.

8. Meguro T, Hong C, Asai K, Takagi G, McKinsey TA, Olson EN, Vatner SF. Cyclosporine attenuates pressure-overload hypertrophy in mice while enhancing susceptibility to decompensation and heart failure. Circ Res. 1999;84:735–740.

9. Yatani A, Honda R, Tymitz KM, Lalli MJ, Molkentin JD. Enhanced Ca^{2+} channel currents in cardiac hypertrophy induced by activation of calcineurin-dependent pathway. *J Mol Cell Cardiol.* 2001;33:249–259.

10. Clerk A, Pham FH, Fuller SJ, Sahai E, Aktories K, Marais R, Marshall C, Sugden PH. Regulation of mitogen-activated protein kinases in cardiac myocytes through the small G protein Rac1. *Mol Cell Biol.* 2001;21: 1173–1184.

11. Nemoto S, Sheng Z, Lin A. Opposing effects of Jun kinase and p38 mitogen-activated protein kinases on cardiomyocyte hypertrophy. *Mol Cell Biol.* 1998;18:3518–3526.

12. Rongen GA, Lenders JW, Lambrou J, Willemsen JJ, Van Belle H, Thien T, Smits P. Presynaptic inhibition of norepinephrine release from sympathetic nerve endings by endogenous adenosine. *Hypertension.* 1996;27: 933–938.

13. Stowe DF, O'Brien WC, Chang D, Knop CS, Kampine JP. Reversal of endothelin-induced vasoconstriction by endothelium-dependent and -independent vasodilators in isolated hearts and vascular rings. *J Cardiovasc Pharmacol.* 1997;29:747–754.

14. Taddei S, Arzilli F, Arrighi P, Salvetti A. Dipyridamole decreases circulating renin-angiotensin system activity in hypertensive patients. *Am J Hypertens.* 1992;5:29–31.

15. Wagner DR, McTiernan C, Sanders VJ, Feldman AM. Adenosine inhibits lipopolysaccharide-induced secretion of tumor necrosis factor-α in the failing human heart. *Circulation.* 1998;97:521–524.

16. Meyer TE, Chung ES, Perlini S, Norton GR, Woodiwiss AJ, Lorbar M, Fenton RA, Dobson JG Jr. Antiadrenergic effects of adenosine in pressure overload hypertrophy. *Hypertension.* 2001;37:862–868.

17. Dubey RK, Gillespie DG, Mi Z, Jackson EK. Exogenous and endogenous adenosine inhibits fetal calf serum-induced growth of rat cardiac fibroblasts: role of A$_{2B}$ receptors. *Circulation.* 1997;96:2656–2666.

18. Funaya H, Kitakaze M, Node K, Minamino T, Komamura K, Hori M. Plasma adenosine levels increase in patients with chronic heart failure. *Circulation.* 1997;95:1363–1365.

19. Kitakaze M, Minamino T, Node K, Koretsune Y, Komamura K, Funaya H, Kuzuya T, Hori M. Elevation of plasma adenosine levels may attenuate the severity of chronic heart failure. *Cardiovasc Drugs Ther.* 1998;12:307–309.

20. Simpson P, McGrath A, Savion S. Myocyte hypertrophy in neonatal rat heart cultures and its regulation by serum and by catecholamines. *Circ Res.* 1982;51:787–801.

21. Liao Y, Ishikura F, Beppu S, Asakura M, Takashima S, Asanuma H, Sanada S, Kim J, Ogita H, Kuzuya T, Node K, Kitakaze M, Hori M. Echocardiographic assessment of LV hypertrophy and function in aortic-banded mice: necropsy validation. *Am J Physiol Heart Circ Physiol.* 2002;282:H1703–H1708.

22. Ding B, Price RL, Borg TK, Weinberg EO, Halloran PF, Lorell BH. Pressure overload induces severe hypertrophy in mice treated with cyclosporine, an inhibitor of calcineurin. *Circ Res.* 1999;84:729–734.

23. Choi DJ, Koch WJ, Hunter JJ, Rockman HA. Mechanism of β-adrenergic receptor desensitization in cardiac hypertrophy is increased β-adrenergic receptor kinase. *J Biol Chem.* 1997;272:17223–17229.

24. Kitakaze M, Node K, Asanuma H, Takashima S, Sakata Y, Asakura M, Sanada S, Shinozaki Y, Mori H, Kuzuya T, Hori M. Protein tyrosine kinase is not involved in the infarct size-limiting effect of ischemic preconditioning in canine hearts. *Circ Res.* 2000;87:303–308.

25. Brown R, Ollerstam A, Johansson B, Skott O, Gebre-Medhin S, Fredholm B, Persson AE. Abolished tubuloglomerular feedback and increased plasma renin in adenosine A$_1$ receptor-deficient mice. *Am J Physiol Regul Integr Comp Physiol.* 2001;281:R1362–R1367.

26. Brede M, Wiesmann F, Jahns R, Hadamek K, Arnolt C, Neubauer S, Lohse MJ, Hein L. Feedback inhibition of catecholamine release by two different α_2-adrenoceptor subtypes prevents progression of heart failure. *Circulation.* 2002;106:2491–2496.

27. Snyder DL, Wang W, Pelleg A, Friedman E, Horwitz J, Roberts J. Effect of aging on A$_1$-adenosine receptor-mediated inhibition of norepinephrine release in the rat heart. *J Cardiovasc Pharmacol.* 1998;31:352–358.

28. Zhao Z, Rivkees SA. Inhibition of cell proliferation in the embryonic myocardium by A$_1$ adenosine receptor activation. *Dev Dyn.* 2001;221: 194–200.

29. Pepperl DJ, Shah-Basu S, VanLeeuwen D, Granneman JG, MacKenzie RG. Regulation of RGS mRNAs by cAMP in PC12 cells. *Biochem Biophys Res Commun.* 1998;243:52–55.

30. Gottlieb SS, Brater DC, Thomas I, Havranek E, Bourge R, Goldman S, Dyer F, Gomez M, Bennett D, Ticho B, Beckman E, Abraham WT. BG9719 (CVT-124), an A$_1$ adenosine receptor antagonist, protects against the decline in renal function observed with diuretic therapy. *Circulation.* 2002;105:1348–1353.

31. Hill JA, Karimi M, Kutschke W, Davisson RL, Zimmerman K, Wang Z, Kerber RE, Weiss RM. Cardiac hypertrophy is not a required compensatory response to short-term pressure overload. *Circulation.* 2000;101: 2863–2869.

32. Esposito G, Rapacciuolo A, Naga Prasad SV, Takaoka H, Thomas SA, Koch WJ, Rockman HA. Genetic alterations that inhibit in vivo pressure-overload hypertrophy prevent cardiac dysfunction despite increased wall stress. *Circulation.* 2002;105:85–92.

PACSIN3 Binds ADAM12/Meltrin α and Up-regulates Ectodomain Shedding of Heparin-binding Epidermal Growth Factor-like Growth Factor*

Seiji Mori‡, Motonari Tanaka§, Daisuke Nanba§, Eiji Nishiwaki¶, Hiroshi Ishiguro¶, Shigeki Higashiyama§‖, and Nariaki Matsuura‡

From the ‡Department of Molecular Pathology, School of Allied Health Science, Osaka University Faculty of Medicine, 1-7 Yamadaoka, Suita, Osaka 565-0871, the §Department of Medical Biochemistry, Ehime University School of Medicine, Shitsukawa, Shigenobu-cho, Onsen-gun, Ehime 791-0295, and the ¶Carna Biosciences Inc., Kobe 650-8543, Japan

A disintegrin and metalloprotease 12 (ADAM12/meltrin α) is a key enzyme implicated in the ectodomain shedding of membrane-anchored heparin-binding epidermal growth factor (EGF)-like growth factor (proHB-EGF)-dependent epidermal growth factor receptor (EGFR) transactivation. However, the activation mechanisms of ADAM12 are obscure. To determine how ADAM12 is activated, we screened proteins that bind to the cytoplasmic domain of ADAM12 using a yeast two-hybrid system and identified a protein called PACSIN3 that contains a Src homology 3 domain. An analysis of interactions between ADAM12 and PACSIN3 using glutathione S-transferase fusion protein revealed that a proline-rich region (amino acid residues 829–840) of ADAM12 was required to bind PACSIN3. Furthermore, co-immunoprecipitation and co-localization analyses of ADAM12 and PACSIN3 proteins also revealed their interaction in mammalian cells expressing both of them. The overexpression of PACSIN3 in HT1080 cells enhanced 12-O-tetradecanoylphorbol-13-acetate (TPA)-induced proHB-EGF shedding. Furthermore, knockdown of endogenous PACSIN3 by small interfering RNA in HT1080 cells significantly attenuated the shedding of proHB-EGF induced by TPA and angiotensin II. Our data indicate that PACSIN3 has a novel function as an up-regulator in the signaling of proHB-EGF shedding induced by TPA and angiotensin II.

The transactivation of epidermal growth factor receptor (EGFR)[1] by G-protein-coupled receptor (GPCR) agonists is a critical element in various responses of diverse cell types including fibroblasts, keratinocytes, astrocytes, and smooth mus-

---

‖ To whom correspondence should be addressed: Dept. of Medical Biochemistry, Ehime University School of Medicine, Shitsukawa, Shigenobu-cho, Onsen-gun, Ehime 791-0295, Japan. Tel.: 81-89-960-5253; Fax: 81-89-960-5256; E-mail: shigeki@m.ehime-u.ac.jp.

[1] The abbreviations used are: EGFR, EGF receptor; EGF, epidermal growth factor; HB-EGF, heparin-binding EGF-like growth factor; GPCR, G-protein-coupled receptor; TPA, 12-O-tetradecanoylphorbol-13-acetate; SH3, Src homology 3; siRNA, small interfering RNA; HA, hemagglutinin; AP, alkaline phosphatase; GST, glutathione S-transferase; CBB, Coomassie Brilliant Blue; ADAM, a disintegrin and metalloprotease.

cle cells (1, 2). A novel mechanistic concept of the EGFR transactivation-signaling pathway involves the proteolytic release of heparin-binding EGF-like growth factor (HB-EGF) at the surface of cells stimulated with GPCR agonists (3). HB-EGF is a member of the EGF family that directly binds EGFR and thereby enhances its phosphorylation, resulting in cell growth and differentiation (4). Like other members of the EGF family, HB-EGF is synthesized as a membrane-anchored form (proHB-EGF) and then proteolytically processed to become a bioactive soluble form, a process that is called ectodomain shedding. The ectodomain shedding of proHB-EGF is an important post-translational modification that converts a tethered insoluble juxtacrine growth factor into a soluble ligand leading to the autocrine or paracrine activation of EGFR.

Studies of GPCR mitogenic signaling have proven that EGFR transactivation is dependent on HB-EGF in smooth muscle cells (2), cardiac endothelial cells (5), and cardiomyocytes (6), as well as in various pathological processes such as cardiac hypertrophy (6), chronic active gastritis associated with Helicobacter pylori (7), and cystic fibrosis (8).

Growing evidence points to a disintegrin and metalloproteases (ADAMs) as key enzymes of proHB-EGF shedding in EGFR transactivation signaling. All ADAMs have an extracellular portion with a metalloprotease domain, a transmembrane region and a cytoplasmic tail, and several ADAMs have metalloprotease activity. Lemjabbar and Basbaum (8) described that stimulation of platelet-activating factor receptor transactivated EGFR through the shedding of proHB-EGF by ADAM10 in the human epithelial cell line HM3. Yan et al. (9) demonstrated that stimulation with the bombesin receptor transactivated EGFRs via the ADAM10-dependent cleavage of proHB-EGF in COS-7 cells. We also identified ADAM12 as a specific enzyme that catalyzes proHB-EGF shedding in EGFR transactivation by GPCR agonists, such as phenylephrine, endothelin-1, and angiotensin II causing cardiac hypertrophy (6). Izumi et al. (10) showed that ADAM9 is involved in TPA-induced shedding of HB-EGF in Vero-H cells when protein kinase Cδ is activated. However, Weskamp et al. (11) found that TPA-stimulated shedding of HB-EGF is unaffected in embryonic fibroblasts derived from mice lacking ADAM9. Moreover, Kurisaki et al. (12) discovered that TPA-induced proHB-EGF shedding is completely abrogated in embryonic fibroblasts derived from mice lacking ADAM12, arguing against an essential role for ADAM9 in proHB-EGF shedding.

These reports indicate that the ectodomain shedding of EGFR ligands, especially of proHB-EGF, is central to GPCR and EGFR communication. However, the underlying mechanisms of the ligand shedding-dependent EGFR transactivation

Regulation of HB-EGF Shedding by ADAM12-PACSIN3 Interaction

A

1. pBTM116- pACT2 PACSIN3
2. pBTM116 ADAM12- pACT2 PACSIN3
3. pBTM116 ADAM12-pACT2

B

PACSIN3

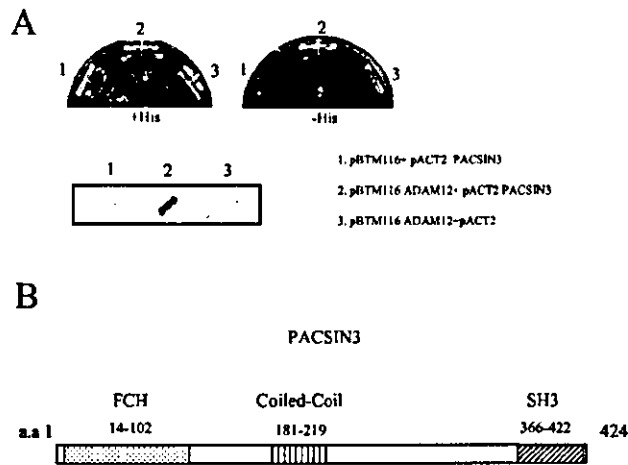| FCH	Coiled-Coil	SH3	
a.a 1	14-102	181-219	366-422	424

FIG. 1. **Interaction of PACSIN3 with cytoplasmic tails of ADAM12 in yeast two-hybrid system.** *A*, yeast strain L40 was co-transformed with prey plasmid pACT2-PACSIN3 together with bait plasmid encoding ADAM12 cytoplasmic domain or control plasmid pBTM116. Bait-prey interactions were assayed in co-transformed yeast by measuring growth without histidine or β-galactosidase production. *B*, schematic representation of PACSIN3. *a.a.*, amino acid.

pathway are largely unknown. Thus, elucidation of the regulatory mechanisms of ADAMs is essential to understand the ligand shedding-dependent EGFR transactivation pathway. The present study focuses on ADAM12, which is involved in TPA or angiotensin II induced HB-EGF shedding and EGFR transactivation. ADAM12 has several Src homology 3 (SH3) domain-binding motifs, (R/K)XXPXXP or PXXPX(R/K) (13) in its cytoplasmic tails, indicating that ADAM12 probably interacts with signaling molecules containing SH3 domains. Therefore, we performed a yeast two-hybrid screening to identify proteins that bind ADAM12 cytoplasmic tails. We found that a protein containing an SH3 domain called PACSIN3 is required for the proHB-EGF shedding induced by TPA and angiotensin II.

EXPERIMENTAL PROCEDURES

Expression Vectors and Small Interfering RNA (siRNA)—The yeast expression plasmid encoding the GAL4 DNA-binding domain fused to the human ADAM12 cytoplasmic domain was constructed by inserting ADAM12 cytoplasmic domain complementary DNA (cDNA) into EcoRI and SalI sites in the multiple cloning sites of the pBTM116 vector (Clontech). We similarly constructed yeast expression plasmids encoding GAL4 DNA-binding domain fused to human ADAM9, ADAM10, ADAM15, ADAM17, and ADAM19 cytoplasmic domains. We prepared an adenovirus carrying a gene encoding FLAG epitope-tagged ADAM12 as described (6). ADAM12 full-length was cloned into the pEGFP-N1 vector (Clontech). The cytoplasmic domain of ADAM12 and its truncated regions were cloned into the pGEX4T-1 vector (Amersham Biosciences). PACSIN3 full-length and truncated (ΔSH3, 1–362 amino acids) cDNAs isolated from a human heart cDNA library by the polymerase chain reaction (PCR) were introduced below the hemagglutinin (HA) sequence into BamHI and NotI sites among the multiple cloning sites of the pcDNA3.1 mammalian expression vector (Invitrogen). PACSIN3 full-length cDNA was also cloned into the pGEX4T-1 vector. The siRNA duplexes were chemically synthesized and purified by Dharmacon Research Inc. The PACSIN3 target sequence 5'-AAGAGGCT-GAAGGAGGTTGAG-3' was selected for PACSIN3 knockdown. This sequence was not substantially similar to any other sequence in the NCBI data base. Scramble siRNA directed against 5'-GCGCGCUUU-GUAGGAUUCG-3' was the negative control. No mammalian mRNAs contained this sequence in the NCBI data base.

Yeast Two-hybrid Screening—Yeast strain L40 containing pBTM116-ADAM12-ΔCyto was selected on synthetic complete medium lacking tryptophan. A human heart cDNA library in pACT2 was introduced into the transformant, and then yeast cells were plated onto synthetic complete medium lacking tryptophan, leucine, and histidine in the presence of 3.5 mM 3-aminotriazole. We assayed the β-galacto-
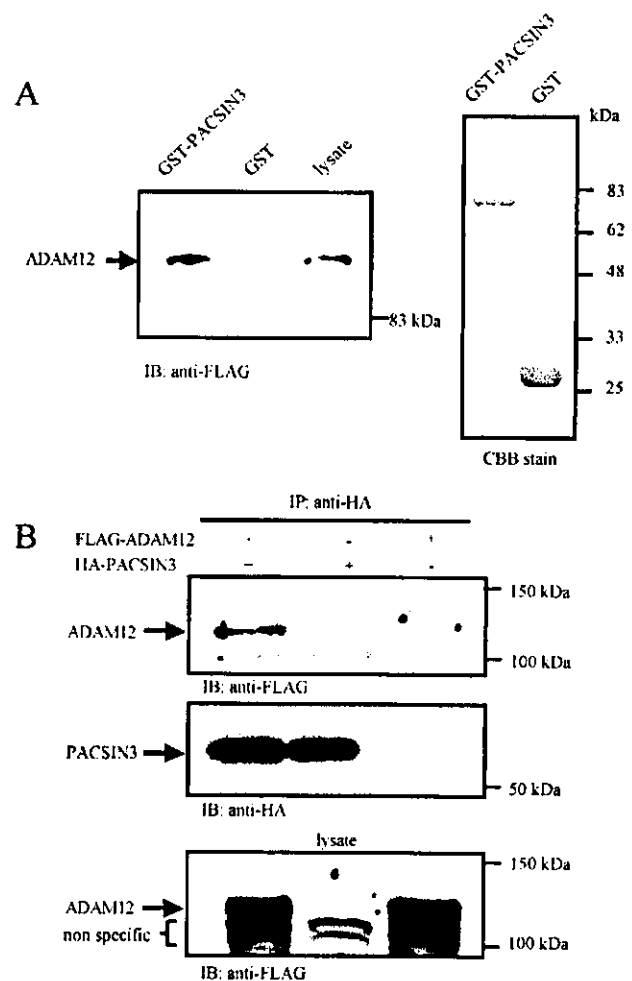
A

IB: anti-FLAG

CBB stain

B

FLAG-ADAM12
HA-PACSIN3

IB: anti-FLAG

IB: anti-HA

IB: anti-FLAG

FIG. 2. **Interaction of ADAM12 with PACSIN3.** *A*, binding of ADAM12 to PACSIN3 *in vitro*. Extracts prepared from HT1080 cells infected with adenovirus vector encoding FLAG-ADAM12 were incubated with either GST or GST-fused PACSIN3 immobilized onto glutathione-conjugated resin. Proteins bound to the resin were separated by SDS-PAGE and either immunoblotted or stained with CBB. *Left*, immunoblotting using anti-FLAG antibody. Arrow, FLAG-ADAM12. *Right*, Purified GST and GST-PACSIN3 stained with CBB. *B*, association of ADAM12 with PACSIN3 in HT1080 cells. HT1080/HA-PACSIN3 cells were infected with or without adenovirus vector encoding FLAG-ADAM12 and HT1080/HA infected with adenovirus vector encoding FLAG-ADAM12 were immunoprecipitated using anti-HA antibody (*middle panel*). Co-immunoprecipitated ADAM12 was detected by immunoblotting using anti-FLAG antibody (*top panel*). Lower panel, FLAG-ADAM12 in cell lysates detected by anti-FLAG antibody.

sidase activity of transformants grown on the dropout plates at 30 °C for 3–7 days. Library plasmid DNA was recovered by transformation into *Escherichia coli* HB101 cells and sequenced.

Cell Culture and Transfection—HT1080 cells were cultured in Eagle's minimum essential medium supplemented with 0.1 mM non-essential amino acids and 10% fetal bovine serum at 37 °C in 5% CO_2. HT1080 cells stably expressing one of HA-tagged PACSIN3 (HA-PAC-SIN3), HA-tagged PACSIN3-ΔSH3 (HA-PACSIN3-ΔSH3), alkaline phosphatase (AP)-tagged proHB-EGF (proHB-EGF-AP) (14), or both proHB-EGF-AP and angiotensin type I (AT1) receptor were also maintained under the same conditions except for the presence of 200 μg/ml hygromycin B. Cells at 80–90% confluence were transfected with mammalian expression vectors using LipofectAMINE 2000 (Invitrogen) according to the manufacturer's instructions or infected with adenovirus at 50 multiplicity of infection and then incubated for 40 h.

Preparation of Cell Extracts—Cells were washed with phosphate-buffered saline and lysed in 50 mM Tris-HCl (pH 7.4) containing 120 mM NaCl, 0.5% Nonidet P-40, 1 mM EDTA, 1 mM phenylmethylsulfonyl fluoride, 10 mM leupeptin, 1.5 mM pepstatin, 1 mM aprotinin, and 50 mM
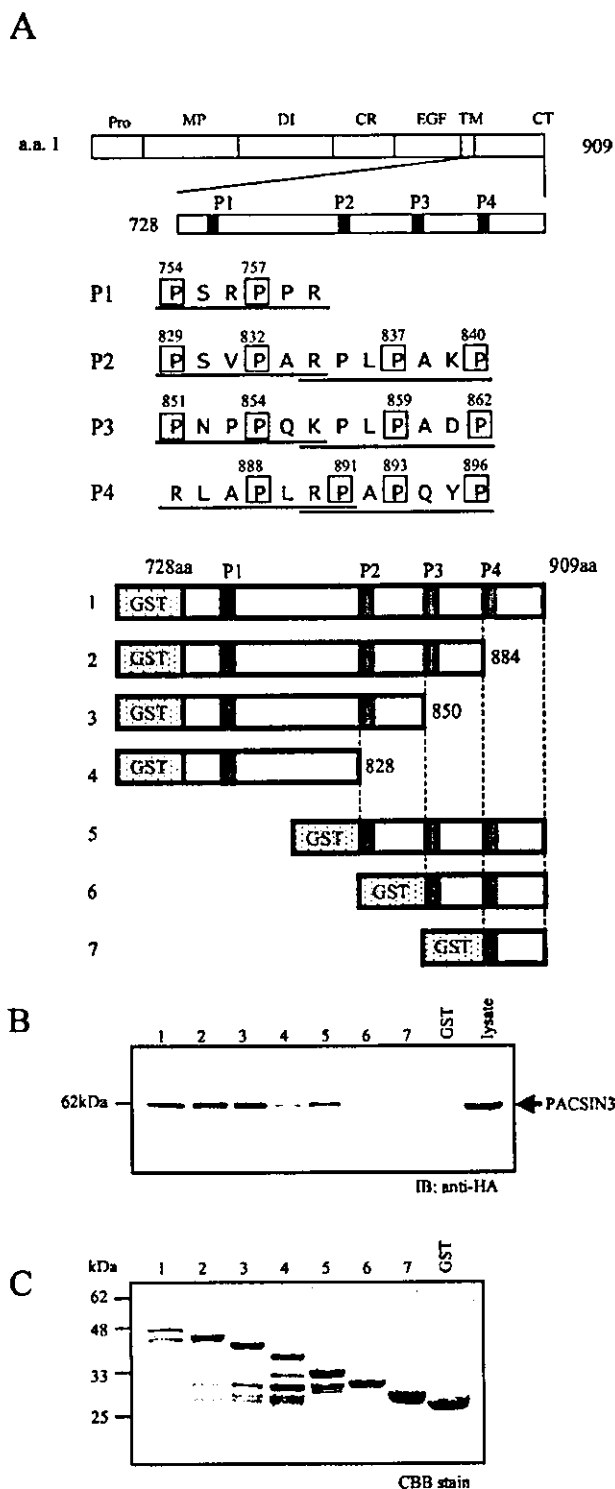
A

B

IB: anti-HA

C

CBB stain

FIG. 3. **Deletion analysis of ADAM12 cytoplasmic domain.** *A,* schematic representation of ADAM12 and cytoplasmic domain deletion mutants. Four proline-rich regions that bind SH3 domain in the cytoplasmic domain of ADAM12 are indicated as P1 to P4. *Pro,* prodomain; *MP,* metalloprotease-like domain; *DI,* disintegrin-like domain; *CR,* cysteine-rich domain; *EGF,* EGF-like repeat domain; *TM,* transmembrane domain; *CT,* cytoplasmic domain. *B,* PACSIN3 binding to deletion mutants. Extracts prepared from HT1080 cells transfected with HA-PACSIN3 were incubated with either GST or with GST fusion proteins immobilized onto glutathione resin. Bound PACSIN3 was detected by immunoblotting using anti-HA antibody. *Arrowhead,* PACSIN3. *C,* GST or GST fusion proteins separated by SDS-PAGE stained with CBB.
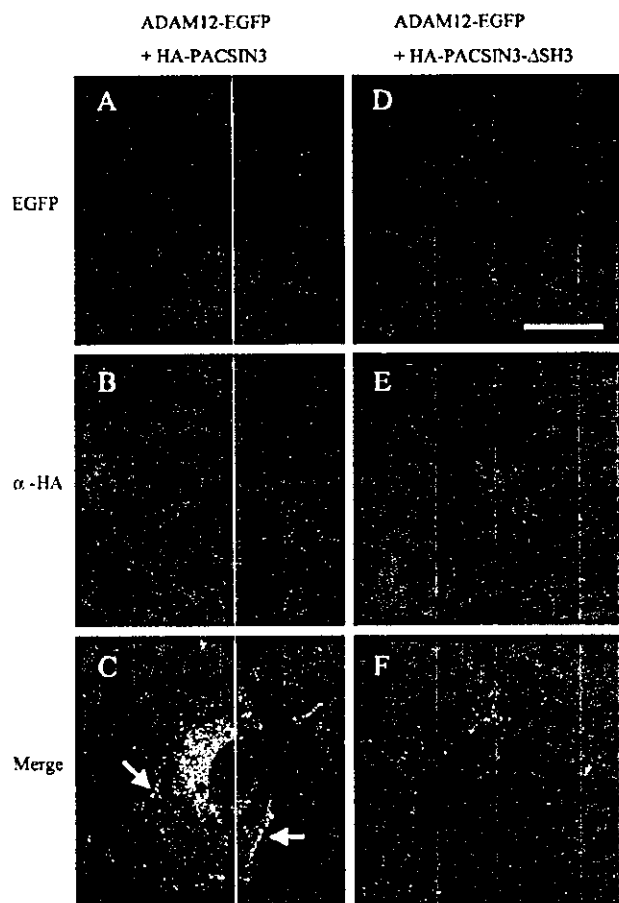
ADAM12-EGFP + HA-PACSIN3   ADAM12-EGFP + HA-PACSIN3-ΔSH3

FIG. 4. **Co-localization of ADAM12 and PACSIN3.** HT1080 cells co-expressing ADAM12-EGFP and either HA-PACSIN3 (*A–C*) or HA-PACSIN3-ΔSH3 (*D–F*) were imaged for EGFP fluorescence (*A, D*) and anti-HA antibody combined with Cy3-conjugated anti-mouse antibody (*B, E*). *C* and *F,* merged images. *Arrows,* ADAM12-EGFP co-localized with HA-PACSIN3 at the plasma membrane. The *white bar* in *D* represents 20 μm.

sodium fluoride (lysis buffer). After centrifugation for 15 min at 12,000 rpm, the supernatant was collected as cell extract.

Pull-down Assay with Immobilized Glutathione S-Transferase (GST) Fusion Proteins—We separated GST and GST-fusion proteins using SDS-PAGE and stained them with Coomassie Brilliant Blue. The proteins were immobilized onto glutathione-Sepharose and exposed to pull-down FLAG-tagged ADAM12 (FLAG-ADAM12) from cell lysates. Cell lysates were incubated with either GST or GST fusion proteins on the resin in 500 μl of the lysis buffer described above with gentle agitation at 4 °C for 4 h. After extensive washing with lysis buffer, bound proteins were released by boiling in SDS-sample buffer, separated by SDS-PAGE, and then immunoblotted.

Immunoprecipitation—The HT1080/HA-PACSIN3 cell lysates were incubated for 2 h with an anti-HA polyclonal antibody (Y11) (Santa Cruz Biotechnology). Protein G-Sepharose (Amersham Biosciences) was added, and the mixture was incubated for 4 h. The immunoprecipitates were collected by centrifugation, washed five times with lysis buffer, resolved by SDS-PAGE, and immunoblotted.

Immunoblot Analysis—Resolved proteins were transferred onto an Immobilon-P membrane (Millipore) and immunoblotted against the following primary antibodies: anti-HA monoclonal antibody (12CA5) (Roche Applied Science), anti-FLAG monoclonal antibody (M2) (Sigma), or anti-PACSIN3 polyclonal antibody raised against GST fusion protein. The secondary antibody was either horseradish peroxidase-conjugated anti-mouse or anti-rabbit antibody (Promega). The immunoreactive proteins were visualized using the ECL detection system (Amersham Biosciences).

Confocal Microscopy—HT1080/HA-PACSIN3 and HT1080/HA-PACSIN3-ΔSH3 cells were transiently transfected with pEGFP-ADAM12.

Thereafter, the cells were fixed with 4% paraformaldehyde, permeabilized using 0.1% Nonidet P-40, and stained with anti-HA monoclonal antibody followed by goat Cy3-conjugated anti-mouse antibody (Jackson ImmunoResearch Laboratories, Inc., West Grove, PA). Fluorescent images were acquired at the resolution of 512 × 512 using a Bio-Rad Radiance 2000 confocal device fitted on a Nikon Eclipse E-600 microscope with a 100 x/1.4 PlanAPO oil-immersion objective. Red and green signals were collected sequentially to avoid bleed through.

Assay of ProHB-EGF-AP Shedding—Cells at 80–90% confluence were transfected with 0.8 μg of siRNA (per well of 24-well plates) and incubated for 40 h. The cells were then incubated for 60 min at 37 °C with 50 nm TPA or 100 nm angiotensin II. Aliquots (100 μl) of conditioned media were transferred to 96-well plates, and AP activity was measured as described previously (14).

RESULTS

Identification of Binding Proteins That Interact with ADAM12 by Yeast Two-hybrid Screening—To identify proteins that interact with the cytoplasmic domain of ADAM12, 3.0 × 10^6 clones of a human heart cDNA library were screened using the yeast two-hybrid system and the ADAM12 cytoplasmic domain as bait. Thirteen positive clones were obtained and sequenced. A homology search in GenBank™ cDNA data bases using the BLAST program revealed that two of the isolated clones overlap with the carboxyl-terminal region of PACSIN3 cDNA. PACSIN3 full-length cDNA was cloned by PCR from a human heart cDNA library, and interaction between PACSIN3 and the cytoplasmic domain of ADAM12 in yeast cells was confirmed by growth under nutritional selection and by β-galactosidase production (Fig. 1A). The domain structure of PACSIN3 has a Fes/CIP4 homology domain in the amino-terminal region, followed by a coiled coil domain and a SH3 domain at the carboxy-terminal region (Fig. 1B) (15).

PACSIN3 Associates with ADAM12 in Vitro and in Vivo—We performed *in vitro* binding assays to confirm that PACSIN3 and ADAM12 interact. FLAG-ADAM12 bound to GST-PACSIN3 fusion protein but not to GST alone in extracts from HT1080 cells expressing FLAG-ADAM12 (Fig. 2A). To further confirm that these two proteins can associate in mammalian cells, FLAG-ADAM12 was transiently expressed in HT1080/HA-PACSIN3 cells. Fig. 2B shows that anti-HA antibody immunoprecipitated HA-PACSIN3 from cell lysates of HT1080 cells transfected with HA-PACSIN3, but not from mock-transfected cell lysates (*middle panel*), and co-immunoprecipitated FLAG-ADAM12, which was detected by the anti-FLAG antibody (*upper panel*). FLAG-ADAM12 expression was detected by anti-FLAG antibody in the lysates of HT1080 cells transfected with FLAG-ADAM12 but not in lysates from mock-transfected HT1080 cells (*lower panel*).

Determination of Cytoplasmic Domain of ADAM12 Required for PACSIN3 Binding—To define the binding site of ADAM12 for PACSIN3, we assayed binding *in vitro* using a series of truncated mutants of the cytoplasmic domain of ADAM12 (Fig. 3, A and C). HA-PACSIN bound to GST-ADAM12-Cyto-1, -2 and -3 equally and to GST-ADAM12-Cyto-4 and -5 to a lesser extent in extracts from HT1080 cells expressing HA-PACSIN3 (Fig. 3B). In contrast, HA-PACSIN3 did not bind to GST-ADAM12-Cyto-6 and -7 (Fig. 3B). These results suggest that P1 (amino acid residues 754–759) and P2 (amino acid residues 829–840) are required for binding to PACSIN3.

Co-localization of ADAM12 and PACSIN3—To determine the intracellular localization of ADAM12 and PACSIN3, EGFP-fused ADAM12 (ADAM12-EGFP) was transiently expressed in HT1080/HA-PACSIN3 or HT1080/HA-PACSIN3-ΔSH3 cells. Fluorescence microscopy revealed that ADAM12-EGFP and HA-PACSIN3 co-localized at intracellular vesicles and at the leading edge of the cell (Fig. 4, A–C). On the other hand, the combination of ADAM12-EGFP and HA-PACSIN3-ΔSH3 (Fig. 4, D–F) did not co-localize.
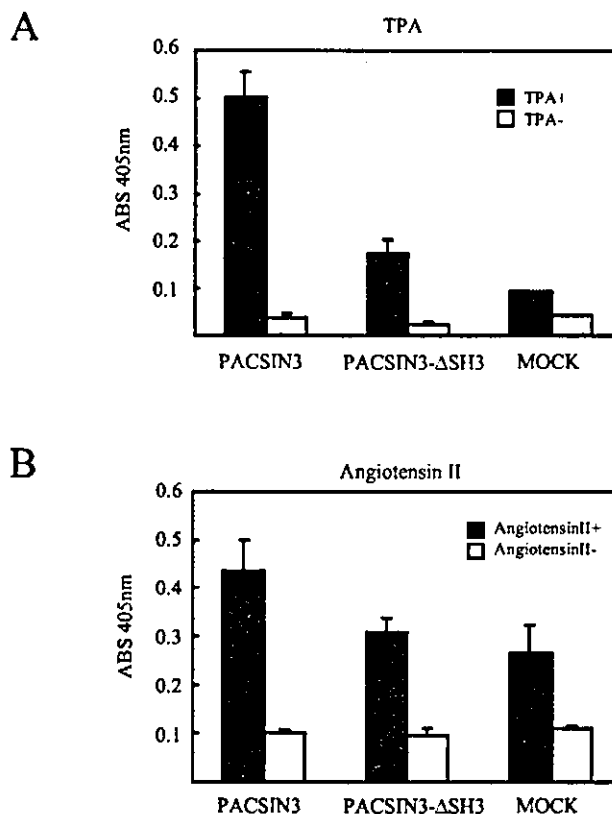
Fig. 5. **Effect of PACSIN3 overexpression on proHB-EGF ectodomain shedding.** AP activity in conditioned media of HT1080/HB-AP, HT1080/HB-AP/HA-PACSIN3, or HT1080/HB-AP/HA-PACSIN3-ΔSH3 cells was measured after incubation with 50 nm TPA (A) or 100 nm angiotensin II (B) for 60 min at 37 °C. Values were normalized using proHB-EGF-AP expression level. Values represent means ± S.E. (n = 4).

Effects of PACSIN3 on Ectodomain Shedding of ProHB-EGF Induced by TPA and Angiotensin II—To investigate the effect of PACSIN3 on the ectodomain shedding of proHB-EGF induced by TPA, PACSIN3 or PACSIN3-ΔSH3 was overexpressed in HT1080/HB-EGF-AP cells. The AP activity in the conditioned medium of each transfectant was then measured after a 60-min incubation with 50 nm TPA. The overexpression of PACSIN3 enhanced TPA-induced proHB-EGF-AP shedding ~5-fold compared with the control, whereas the effect of PACSIN3-ΔSH3 overexpression was quite minimal (Fig. 5A). However, PACSIN3 overexpression did not enhance proHB-EGF-AP shedding induced by angiotensin II to a statistically significant extent (Fig. 5B). To confirm that PACSIN3 functions as an up-regulator of proHB-EGF ectodomain shedding, we destroyed the mRNA using siRNA mediation. To test the effect of PACSIN3-siRNA on knockdown, we estimated the level of endogenous PACSIN3 protein by immunoblotting. We detected less endogenous PACSIN3 protein in the lysate from HT1080 cells transfected with PACSIN3-siRNA than in those transfected with negative control scramble siRNA (Fig. 6A). This result confirmed that PACSIN3-siRNA reduced endogenous PACSIN3 protein levels. We then assessed the effect of PACSIN3-siRNA on the ectodomain shedding of proHB-EGF induced by TPA. HT1080/HB-EGF-AP cells were transfected with Scramble-siRNA or with PACSIN3-siRNA, and AP activity was measured in the same manner as described above.

In addition, proHB-EGF-AP shedding induced by angiotensin II was assayed using HT1080/HB-EGF-AP/AT1 cells. PACSIN3 knockdown mediated by PACSIN3-siRNA attenuated 50
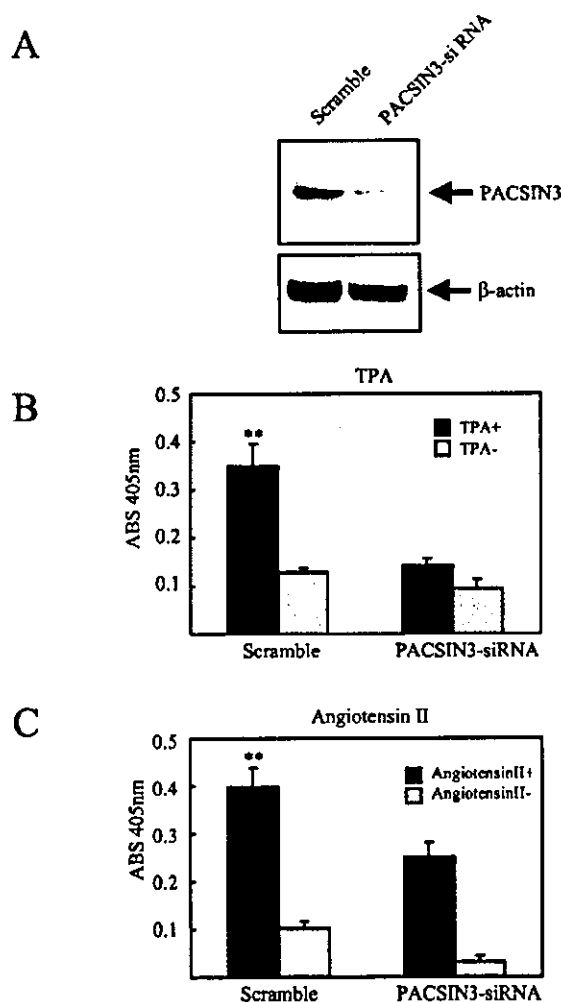
A

B

C

Fig. 6. Knockdown of PACSIN3 by siRNA. *A*, immunoblot analysis. HT1080 cell lysates were immunoblotted using anti-PACSIN3 antibody. *B* and *C*, effect of PACSIN3 knockdown on shedding of proHB-EGF induced by 50 nM TPA (*B*) and 100 nM angiotensin II (*C*). AP activity in conditioned medium of HT1080/HB-AP or HT1080/HB-AP/AT1 cells transfected with siRNA was measured after incubation with 50 nM TPA or 100 nM angiotensin II for 60 min at 37 °C, respectively. Values represent means ± S.E. ($n = 4$). **, $p < 0.01$ for scramble *versus* siRNA with TPA or angiotensin II.

and 45% of the control levels of TPA- and angiotensin II-induced proHB-EGF-AP shedding, respectively (Fig. 6, *B* and *C*).

Specificity of PACSIN3 Binding to ADAMs—We studied the specificity of ADAMs for PACSIN3 association. Fig. 7 shows the binding affinity of the cytoplasmic domains of various ADAM proteins for PACSIN3 determined by the yeast two-hybrid system. The cytoplasmic domains of ADAMs 9, 10, 12, 15, and 19 interacted with PACSIN3 but not those of ADAM17 both in yeast growth (Fig. 7*A*) and β-galactosidase assays (Fig. 7*B*).

DISCUSSION

The current study investigated the regulatory mechanisms of ADAM-dependent proHB-EGF shedding induced by TPA or GPCR agonists. We then focused on ADAM12 that has recently been identified as a shedding enzyme involved in proHB-EGF. Since the cytoplasmic tail of human ADAM12 has four class I (R/K)XXPXXP and three class II PXXPX(R/K) SH3 domain-binding motifs grouped into four proline-rich regions (Fig. 3*A*), ADAM12 probably interacts with several signaling molecules
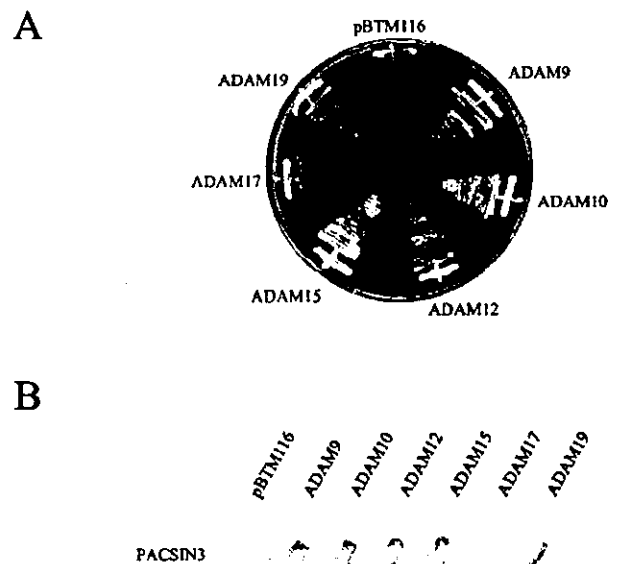
A

B

Fig. 7. Interaction of PACSIN3 with cytoplasmic tails of several ADAMs. Yeast strain L40 was co-transformed with prey plasmid pACT2-PACSIN3 together with bait plasmids encoding cytoplasmic domains of ADAMs or control plasmid pBTM116. Co-transformed yeasts were assayed for bait-prey interactions by determining growth without histidine (*A*) or β-galactosidase production (*B*).

containing SH3 domains. Yeast two-hybrid screening using the cytoplasmic domain of ADAM12 as bait resulted in the isolation of PACSIN3 characterized by Fes/CIP4 homology and SH3 domains in the amino- and carboxyl-terminal regions, respectively. PACSIN3 is supposed to be a cytoplasmic molecule involved in endocytosis. For example, PACSIN3 binds endocytic proteins such as dynamin, synaptojanin 1, and N-WASP *in vitro*, and PACSIN3 overexpression blocks endocytosis (16).

ADAM12 interacts with signaling molecules containing an SH3 domain such as Src and the p85α regulatory subunit of phosphatidylinositol 3-kinase, and the binding sites for these proteins are located in P2, and in P2 or P4 of the ADAM12 cytoplasmic tail, respectively (17–19). Binding assays using a series of truncated mutants mapped the PACSIN3-binding sites to P1 and P2 in ADAM12 cytoplasmic tail. These findings suggest that the PACSIN3-binding sites are shared by several proteins containing SH3 domains, although whether the binding of these proteins to ADAM12 cytoplasmic tail is exclusive remains unknown.

Microscopy revealed that HA-PACSIN3 was diffused throughout the cytoplasm and partially localized in the plasma membrane where some endogenous ADAM12 also resides. On the other hand, ADAM12-EGFP was intracellularly distributed in a vesicle-like manner, consistent with other reports indicating that exogenous ADAM12 is localized mainly in the endoplasmic reticulum, trans-Golgi networks, and partially in the plasma membrane (20, 21). HA-PACSIN3 co-localized with ADAM12-EGFP in the plasma membrane, suggesting that PACSIN3 associates with correctly transported ADAM12 in the plasma membrane. Our findings are also supported by the notion that mutant PACSIN3-ΔSH3 do not co-localize with wild type ADAM12, and previously reported ADAM13 binds to and co-localize with PACSIN2 (22).

We demonstrated that PACSIN3 knockdown by siRNA in HT1080 cells partially attenuated the shedding of proHB-EGF induced by TPA and angiotensin II. Thus, PACSIN3 seems necessary, but alone is insufficient, to regulate the signaling pathway of the ectodomain shedding of HB-EGF induced by

Regulation of HB-EGF Shedding by ADAM12-PACSIN3 Interaction

both TPA and by angiotensin II. In addition, PACSIN-like molecules might be involved in regulating the ectodomain shedding of proHB-EGF induced by TPA and angiotensin II. We also question whether PACSIN3 regulates the ectodomain shedding of proHB-EGF induced by other GPCR.

PACSIN3 can interact with the cytoplasmic tails of ADAM9, ADAM10, ADAM15, and ADAM19 as well as with those of ADAM12 (Fig. 7), suggesting that PACSIN3 widely regulates ADAM-dependent post-translational modification. The physiological significance of interactions between PACSIN3 and these ADAMs, however, remains obscure.

We postulated that PACSIN3 plays a physiological role as a binding partner of ADAM12 in the signaling pathway of proHB-EGF shedding induced by GPCR agonists. Further analyses will clarify the signaling pathway from GPCRs to the processing of proHB-EGF leading to EGFR transactivation.

REFERENCES

1. Daub, H., Wallasch, C., Lankenau, A., Herrlich, A., and Ullrich, A. (1997) *EMBO J.* **16**, 7032–7044
2. Eguchi, S., Numaguchi, K., Iwasaki, H., Matsumoto, T., Yamakawa, T., Utsunomiya, H., Motley, E. D., Kawakatsu, H., Owada, K. M., Hirata, Y., Marumo, F., and Inagami, T. (1998) *J. Biol. Chem.* **273**, 8890–8896
3. Prenzel, N., Zwick, E., Daub, H., Leserer, M., Abraham, R., Wallasch, C., and Ullrich, A. (1999) *Nature* **402**, 884–888
4. Higashiyama, S., Lau, K., Besner, G. E., Abraham, J. A., and Klagsbrun, M. (1992) *J. Biol. Chem.* **267**, 6205–6212
5. Fujiyama, S., Matsubara, H., Nozawa, Y., Maruyama, K., Mori, Y., Tsutsumi, Y., Masaki, H., Uchiyama, Y., Koyama, Y., Nose, A., Iba, O., Tateishi, E., Ogata, N., Jyo, N., Higashiyama, S., and Iwasaka, T. (2001) *Circ. Res.* **88**, 22–29
6. Asakura, M., Kitakaze, M., Takashima, S., Liao, Y., Ishikura, F., Yoshinaka, T., Ohmoto, H., Node, K., Yoshino, K., Ishiguro, H., Asanuma, H., Sanada, S., Matsumura, Y., Takeda, H., Beppu, S., Tada, M., Hori, M., and Higashiyama, S. (2002) *Nat. Med.* **8**, 35–40
7. Keates, S., Sougioultzis, S., Keates, A. C., Zhao, D., Peek, R. M., Jr., Shaw, L. M., and Kelly, C. P. (2001) *J. Biol. Chem.* **276**, 48127–48134
8. Lemjabbar, H., and Basbaum, C. (2002) *Nat. Med.* **8**, 41–46
9. Yan, Y., Shirakabe, K., and Werb, Z. (2002) *J. Cell Biol.* **158**, 221–226
10. Izumi, Y., Hirata, M., Hasuwa, H., Iwamoto, R., Umata, T., Miyado, K., Tamai, Y., Kurisaki, T., Sehara-Fujisawa, A., Ohno, S., and Mekada, E. (1998) *EMBO J.* **17**, 7260–7272
11. Weskamp, G., Cai, H., Brodie, T. A., Higashiyama, S., Manova, K., Ludwig, T., and Blobel, C. P. (2002) *Mol. Cell Biol.* **22**, 1537–1544
12. Kurisaki, T., Masuda, A., Sudo, K., Sakagami, J., Higashiyama, S., Matsuda, Y., Nagabukuro, A., Tsuji, A., Nabeshima, Y., Asano, M., Iwakura, Y., and Sehara-Fujisawa, A. (2003) *Mol. Cell Biol.* **23**, 55–61
13. Kay, B. K., Williamson, M. P., and Sudol, M. (2000) *FASEB J.* **14**, 231–241
14. Tokumaru, S., Higashiyama, S., Endo, T., Nakagawa, T., Miyagawa, J. I., Yamamori, K., Hanakawa, Y., Ohmoto, H., Yoshino, K., Shirakata, Y., Matsuzawa, Y., Hashimoto, K., and Taniguchi, N. (2000) *J. Cell Biol.* **151**, 209–220
15. Sumoy, L., Pluvinet, R., Andreu, N., Estivill, X., and Escarceller, M. (2001) *Gene (Amst.)* **262**, 199–205
16. Modregger, J., Ritter, B., Witter, B., Paulsson, M., and Plomann, M. (2000) *J. Cell Sci.* **113**, 4511–4521
17. Suzuki, A., Kadota, N., Hara, T., Nakagami, Y., Izumi, T., Takenawa, T., Sabe, H., and Endo, T. (2000) *Oncogene* **19**, 5842–5850
18. Kang, Q., Cao, Y., and Zolkiewska, A. (2000) *Biochem. J.* **352**, 883–892
19. Kang, Q., Cao, Y., and Zolkiewska, A. (2001) *J. Biol. Chem.* **276**, 24466–24472
20. Kadota, N., Suzuki, A., Nakagami, Y., Izumi, T., and Endo, T. (2000) *J. Biochem. (Tokyo)* **128**, 941–949
21. Hougaard, S., Loechel, F., Xu, X., Tajima, R., Albrechtsen, R., and Wewer, U. M. (2000) *Biochem. Biophys. Res. Commun.* **275**, 261–267
22. Cousin, H., Gaultier, A., Bleux, C., Darribère, T., Alfandari, D. (2000) *Dev. Biol.* **227**, 197–210

Article

Proteolytic release of the carboxy-terminal fragment of proHB-EGF causes nuclear export of PLZF

Daisuke Nanba,[1] Akiko Mammoto,[1] Koji Hashimoto,[2] and Shigeki Higashiyama[1]

[1]Department of Medical Biochemistry and [2]Department of Dermatology, Ehime University School of Medicine, Ehime 791-0295, Japan

Cleavage of membrane-anchored heparin-binding EGF-like growth factor (proHB-EGF) via metalloprotease activation yields amino- and carboxy-terminal regions (HB-EGF and HB-EGF-C, respectively), with HB-EGF widely recognized as a key element of epidermal growth factor receptor transactivation in G protein–coupled receptor signaling. Here, we show a biological role of HB-EGF-C in cells. Subsequent to proteolytic cleavage of proHB-EGF, HB-EGF-C translocated from the plasma membrane into the nucleus. This translocation triggered nuclear export of the transcriptional repressor, promyelocytic leukemia zinc finger (PLZF), which we identify as an HB-EGF-C binding protein. Suppression of cyclin A and delayed entry of S-phase in cells expressing PLZF were reversed by the production of HB-EGF-C. These results indicate that released HB-EGF-C functions as an intracellular signal and coordinates cell cycle progression with HB-EGF.

Introduction

Interreceptor cross-talk has received significant attention recently as an essential element in understanding the increasingly complex signaling networks identified within cells. Transactivation of the epidermal growth factor receptor (EGFR) has been shown to play a crucial role in the signaling by G protein–coupled receptors (GPCRs), cytokine receptors, receptor tyrosine kinases, and integrins to a variety of cellular responses (Hackel et al., 1999; Moghal and Sternberg, 1999). Transactivation of EGFR is mediated, at least in some cases, by the EGFR ligand heparin-binding EGF-like growth factor (HB-EGF), which is cleaved from its membrane-anchored form (proHB-EGF) in a process termed "ecto-domain shedding" (Prenzel et al., 1999).

The proHB-EGF molecule is proteolytically cleaved by "a disintegrin and metalloprotease" (ADAM) 9, 12, 10, or 17 (Izumi et al., 1998; Asakura et al., 2002; Lemjabbar and Basbaum, 2002; Sunnarborg et al., 2002; Yan et al., 2002) to release a soluble form of HB-EGF. This cleavage can be stimulated by treating cells with various agents, including the phorbol ester 12-O-tetradecanoylphorbol-13-acetate (TPA), an activator of PKC (Goishi, et al., 1995). Recent analyses have shown that the processing of proHB-EGF by metalloproteases plays important roles in cutaneous wound healing (Tokumaru et al., 2000) and branching morphogenesis of the submandibular gland (Umeda et al., 2001). Furthermore, the cleavage of proHB-EGF is required for EGFR transactivation by GPCR signaling (Prenzel et al., 1999), which is involved in various biological processes such as cardiac hypertrophy (Asakura et al., 2002), cystic fibrosis (Lemjabbar and Basbaum, 2002), and the mitogenic effects of arachidonic acid metabolites (Chen et al., 2002; Cussac et al., 2002).

Although much has been learned about the functions of extracellular domains produced by ectodomain shedding, very little attention has been paid to the remnant cell-associated domains also created by the processing event. Here, we focus on a biological role played by the carboxy-terminal remnant (HB-EGF-C) produced in parallel with HB-EGF, and characterize it as a novel intracellular signaling molecule acquired posttranslationally. Using fluorescent protein–tagged proHB-EGF and an antibody recognizing the cytoplasmic region of proHB-EGF, we visualized the translocation of HB-EGF-C from the plasma membrane into the nucleus

Abbreviations used in this paper: ADAM, a disintegrin and metalloprotease; EGFR, epidermal growth factor receptor; GPCR, G protein–coupled receptor; HB-EGF, heparin-binding EGF-like growth factor; PLZF, promyelocytic leukemia zinc finger; proHB-EGF, membrane-anchored heparin-binding EGF-like growth factor; TPA, 12-O-tetradecanoylphorbol-13-acetate.
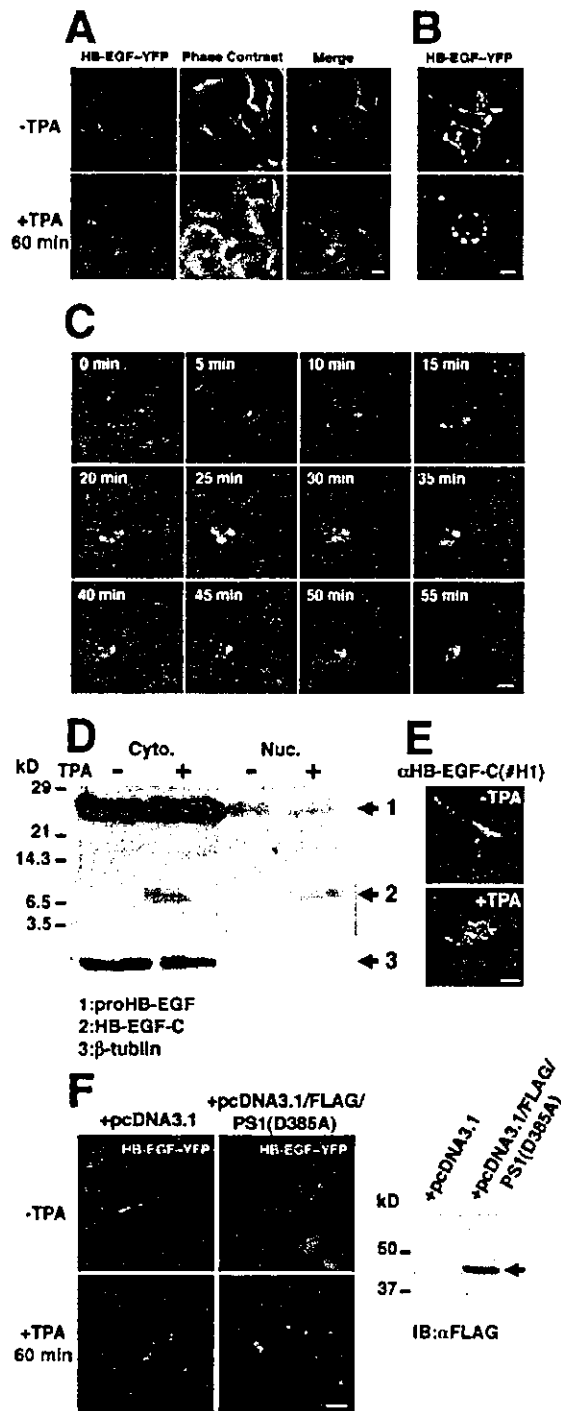
489

after ectodomain shedding of proHB-EGF. Yeast two-hybrid screening resulted in the cloning of an HB-EGF-C binding protein, promyelocytic leukemia zinc finger (PLZF), previously identified as a transcriptional repressor and a negative regulator of the cell cycle. The proteolytic release of HB-EGF-C via metalloprotease activation caused nuclear export of PLZF and reversal of cyclin A suppression and delayed entry of S-phase by PLZF in human fibrosarcoma HT1080 cells. Intracellular trafficking of endogenous HB-EGF-C into the nucleus and the subsequent nuclear export of PLZF after metalloprotease processing of proHB-EGF were also observed in human primary cultured keratinocytes. Thus, our present data provide new insights into the inter- and intracellular communication generated by proHB-EGF processing.

Results

Translocation of HB-EGF-C after TPA-inducible processing

To investigate the behavior of HB-EGF-C after metalloprotease processing of proHB-EGF, we constructed an expression vector encoding a protein in which YFP was fused to the carboxy terminus of proHB-EGF (HB-EGF–YFP). This vector was then transfected into human fibrosarcoma HT1080 cells. HB-EGF–YFP was localized at the plasma membrane of the transfected cells and its ectodomain was released by TPA-inducible proteolysis, as shown previously with wild-type proHB-EGF (unpublished data). In transfected cells treated with TPA for 60 min, fluorescent images revealed the translocation and accumulation of HB-EGF–YFP around the nucleus (Fig. 1, A and B). Time-lapse imaging showed that HB-EGF–YFP began to internalize and accumulate in the cytoplasm 15 min after TPA stimulation, and that a majority of the fluorescent protein had disappeared from the plasma membrane and was observed within the cytoplasm 30 min after TPA stimulation (Fig. 1 C).

Next, we examined the localization of HB-EGF-C by separating cytoplasmic and nuclear fractions from HT1080 cells overexpressing proHB-EGF (HT1080/HB-EGF cells). We used an antibody recognizing the cytoplasmic region of proHB-EGF (#H1) to detect proHB-EGF and HB-EGF-C.

Figure 1. **Translocation of HB-EGF-C after TPA-inducible processing.** (A–C) HT1080 cells were transiently transfected with a plasmid encoding the fusion protein HB-EGF–YFP, in which YFP was fused to the carboxy terminus of proHB-EGF. After 24 h, the subcellular localization of the YFP sequence was visualized with fluorescent microscopy. (A) HB-EGF–YFP in unstimulated cells was observed at the plasma membrane. After stimulation with 100 nM TPA for 60 min, HB-EGF–YFP was absent from the plasma membrane, but detected in the cytoplasm and localized around the nucleus. (B) Localization of the fusion protein was confirmed by confocal microscopy. (C) Representative time-lapse images of HB-EGF–YFP transfected cells are shown every 5 min for up to 55 min after TPA treatment. Note that HB-EGF–YFP at the plasma membrane was translocated into the cytoplasm after TPA stimulation of the cells. (D and E) Accumulation of HB-EGF-C in the nucleus of HT1080 cells overexpressing proHB-EGF (HT1080/HB-EGF cells). (D) Cytoplasmic (Cyto.) and nuclear (Nuc.) fractions were prepared from HT1080/HB-EGF cells (2.0 × 10⁷). After the incubation with or without TPA for 30 min, cells were lysed and immunoblotted using anti-HB-EGF-C antibody (#H1). In addition to a 25-kD band (proHB-EGF), the 6.7-kD band (HB-EGF-C) was detected in the cytoplasmic fraction when cells were treated with TPA. The 6.7-kD band was also detectable in the nuclear fraction after TPA stimulation. (E) Accumulation of HB-EGF-C after TPA treatment was also observed by immunofluorescence microscopy using the #H1 antibody. (F) Transient expression of the amino-terminally FLAG-tagged dominant-negative form of presenilin-1 (D385A) was not altered HB-EGF–YFP translocation after TPA treatment in HT1080 cells (left). Expression of the FLAG-tagged presenilin-1 mutant was confirmed by immunoblotting with anti-FLAG antibody (right, arrow). Bars, 10 μm.

A large amount of proHB-EGF was accumulated in the cytoplasmic fraction, and the band of HB-EGF-C was not observed in cytoplasmic and nuclear fractions without the stimulation (Fig. 1 D). After TPA treatment for 30 min, the 6.7-kD band (the expected size of an HB-EGF-C with transmembrane and cytoplasmic domains of proHB-EGF) was detectable in both cytoplasmic and nuclear fractions of HB-EGF-C after TPA treatment (Fig. 1 E).

To test whether γ-secretase activity is involved with the proteolytic release of HB-EGF-C, we investigated the effect of a dominant-negative mutant of presenilin-1 (PS1 D385A), which reduces γ-secretase activity (Wolfe et al., 1999), on HB-EGF-C translocation after TPA treatment. Transient expression of amino-terminally FLAG-tagged dominant-negative PS1 in HT1080 cells was not altered the HB-EGF–YFP translocation induced by TPA treatment (Fig. 1 F).

Identification of PLZF as a proHB-EGF cytoplasmic domain–binding protein

The translocation of HB-EGF-C after proHB-EGF processing suggested that after proHB-EGF processing, HB-EGF-C could interact with cytoplasmic or nuclear proteins. To identify potential binding proteins of HB-EGF-C, we used yeast two-hybrid cloning and screened a human heart cDNA library using the cytoplasmic region of proHB-EGF (residues 185–208) as bait. Screening of 10^6 transformants yielded 16 positive clones. One of the clones (referred to as clone 3) encoded a carboxy-terminal sequence of PLZF protein (Fig. 2 A), a transcriptional repressor that is localized in the nucleus (Chen et al., 1993; Reid et al., 1995). Immunoprecipitation from COS cells expressing proHB-EGF and CFP-tagged PLZF (CFP-PLZF) revealed that CFP-PLZF was coimmunoprecipitated with the #H1 antibody once the cells were treated with TPA (Fig. 2 B).

To determine the region of PLZF that interacts with HB-EGF-C, we performed a GST pull-down assay. Various FLAG-tagged PLZF derivatives (Fig. 2 C) were incubated with glutathione Sepharose beads containing recombinant HB-EGF-C fused to GST (GST–HB-EGF-C). In agreement with the data obtained from the yeast study, the zinc finger region containing nine zinc finger motifs (the carboxy terminus of PLZF protein) interacted with GST–HB-EGF-C (Fig. 2 D). We further characterized the zinc finger region of PLZF required for interaction with HB-EGF-C. GST–HB-EGF-C pulled down zinc finger 5∼8 motifs (Zn5∼8) efficiently and zinc finger 1∼6 motifs (Zn1∼6) partially, but not the zinc finger 6∼7 motifs (Zn6∼7; Fig. 2 E). However, deletion of Zn6∼7 abrogated the binding of PLZF to GST–HB-EGF-C (Fig. 2 F). These data suggest that the Zn6∼7 region is essential and Zn5∼8 is sufficient for the PLZF-HB-EGF-C interaction.

Nuclear export of PLZF triggered by TPA-inducible ectodomain shedding of proHB-EGF

Next, we examined the subcellular localization of PLZF by using the expression vector encoding CFP-PLZF. This expression vector was transfected into four types of cell lines as follows: HT1080 cells; a stable transfectant of HT1080 expressing proHB-EGF (HT1080/HB-EGF); a stable double transfectant of HT1080 cells expressing proHB-EGF and a metalloprotease domain–deleted mutant of ADAM12

(HT1080/ΔMP-ADAM12/HB-EGF); and a stable transfectant of HT1080 expressing an uncleavable mutant (L148G; Hirata et al., 2001) of proHB-EGF (HT1080/HB-EGF-UC). Endogenous HB-EGF expression was very low in parental HT1080 cells (unpublished data).

CFP-PLZF was predominantly localized in the nucleus in HT1080 cells and in the three transfectants. TPA treatment did not alter the subcellular localization of CFP-PLZF in HT1080 cells. In contrast, TPA treatment for 60 min distributed CFP-PLZF in the entire cytoplasm of HT1080/HB-EGF cells (Fig. 3 A). A previous experiment had revealed that ADAM12 can mediate HB-EGF shedding, and that expression of a dominant-negative (metalloprotease domain–deleted mutant) form of ADAM12 inhibited proHB-EGF processing in HT1080 cells (Asakura et al., 2002). In HT1080/ΔMP-ADAM12/HB-EGF cells, the export of CFP-PLZF from the nucleus to the cytoplasm was not observed after TPA stimulation. Similarly, HT1080/HB-EGF-UC cells did not show the nuclear export of CFP-PLZF despite TPA treatment (Fig. 3 A). Quantitative analyses (see Materials and methods) verified that the number of cells with nuclear-localized CFP-PLZF was reduced by the TPA treatment in HT1080/HB-EGF cells, but not in parental HT1080 cells, HT1080/ΔMP-ADAM12/HB-EGF cells, or HT1080/HB-EGF-UC cells (Fig. 3 C).

Proteolytic cleavage of proHB-EGF induced by TPA yields at least two fragments, HB-EGF and HB-EGF-C. Therefore, we next investigated whether EGFR activation by HB-EGF was involved in triggering the nuclear export of CFP-PLZF in HT1080/HB-EGF cells. HT1080/HB-EGF cells transfected with the plasmid encoding CFP-PLZF were preincubated with 10 μg/ml of EGFR-neutralizing antibody (an amount of antibody sufficient to inhibit tyrosine phosphorylation of EGFR in HT1080/HB-EGF cells after TPA addition; unpublished data). Nuclear export of CFP-PLZF by TPA stimulation was still observed in the presence of the antibody (Fig. 3, B and D). On the other hand, by pretreatment with 10 μM KB-R7785, a metalloprotease inhibitor that blocks proHB-EGF processing by ADAM12 (Asakura et al., 2002), the frequency of the nuclear export of CFP-PLZF after TPA stimulation of HT1080/HB-EGF cells was reduced (Fig. 3, B and D). The export of CFP-PLZF was also inhibited by preincubation of the cells with 10 ng/ml leptomycin B (LMB), a specific inhibitor of CRM1 (designated exportin 1)-dependent nuclear export (Kudo et al., 1999; Fig. 3, B and D). These results indicate that generation of HB-EGF-C by proHB-EGF processing is required for the nuclear export of PLZF.

The GST pull-down analysis indicated that deletion of Zn6∼7 of PLZF abrogated the binding to HB-EGF-C. Therefore, we investigated the nuclear export of CFP-PLZF with deletion of Zn6∼7 (CFPPLZFΔZn6∼7) in HT1080/HB-EGF cells. The frequency of the CFP-PLZFΔZn6∼7 export much decreased as compared with CFP-PLZF after TPA stimulation (Fig. 3, E and F). This result indicates that binding of PLZF to HB-EGF-C is essential for the nuclear export of PLZF.

Translocation and interaction of HB-EGF-C with PLZF precedes nuclear export of PLZF

Next, we performed the simultaneous visualization of proHB-EGF processing and PLZF transport. Processing of
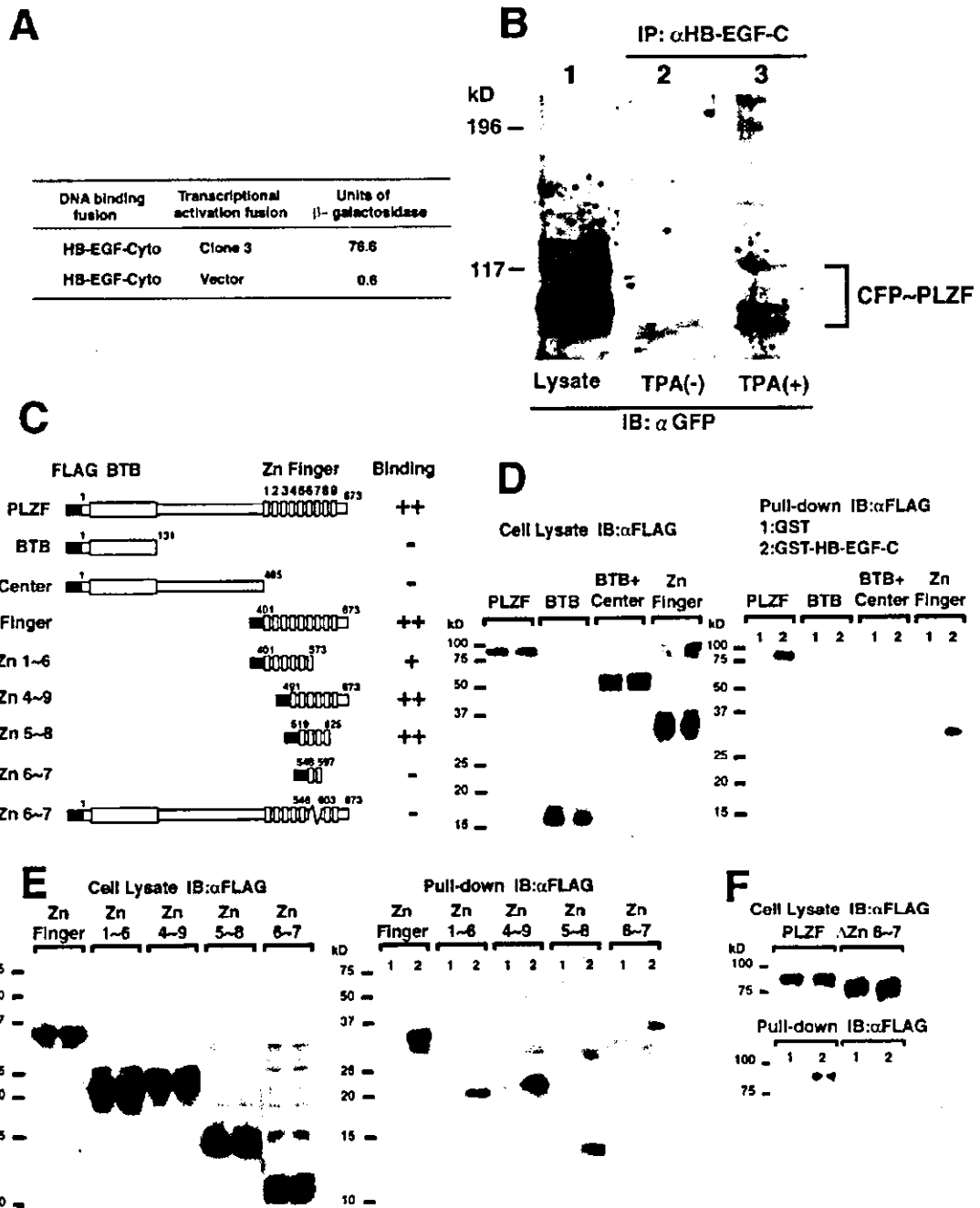
Figure 2.   Identification of PLZF as an HB-EGF-C binding protein. (A) We used the yeast two-hybrid method and screened a human heart cDNA library with the cytoplasmic region of HB-EGF (HB-EGF-Cyto; residues 185–208) as bait. One of the positive clones (clone 3) was identified as encoding a portion of PLZF. (B) COS cells were transiently transfected with a proHB-EGF expression vector and a CFP-PLZF expression vector encoding a fusion protein in which CFP was fused to the amino terminus of PLZF, stimulated for 60 min with TPA, and lysed. Expression of CFP-PLZF was confirmed by immunoblotting of the whole lysate with anti-GFP antibody (lane 1). The lysates were immunoprecipitated with anti-HB-EGF-C antibody (#H1), and the precipitates were immunoblotted with anti-GFP antibody (lanes 2 and 3). Note that the interaction between PLZF and HB-EGF was observed when cells were stimulated with TPA. (C–F) GST pull-down assay. Cell lysates containing the FLAG-tagged PLZF derivatives were incubated with GST (1) or GST–HB-EGF-C (2) beads, and bound proteins were detected by immunoblotting using an anti-FLAG antibody (right). Expression of the derivatives was also confirmed by immunoblotting using an anti-FLAG antibody (left). (C) Schematic diagrams of FLAG-tagged PLZF derivatives. Nine zinc finger motifs in the PLZF protein are numbered from first to ninth. Binding properties of PLZF derivatives to GST–HB-EGF-C is summarized in the right lane of each structure. The binding properties are based on the estimation from the intensity of bands as compared with the control band and are indicated as + + (>50%), + (50–10%), and − (<10%). (D) Full-length PLZF and the fragment containing nine zinc finger motifs (Zn Finger) were bound to GST–HB-EGF-C, but not to GST alone. (E) The fragments consisting of zinc finger motifs 4~9 (Zn4~9) and 5~8 (Zn5~8) were bound to GST–HB-EGF-C stronger than the fragment with zinc finger motifs 1~6 (Zn1~6). The fragment consisting of zinc finger motifs 6~7 (Zn6~7) was not efficient for the interaction. (F) Deletion mutant (ΔZn6~7) showed that the region with Zn6~7 was essential for HB-EGF-C–PLZF interaction.
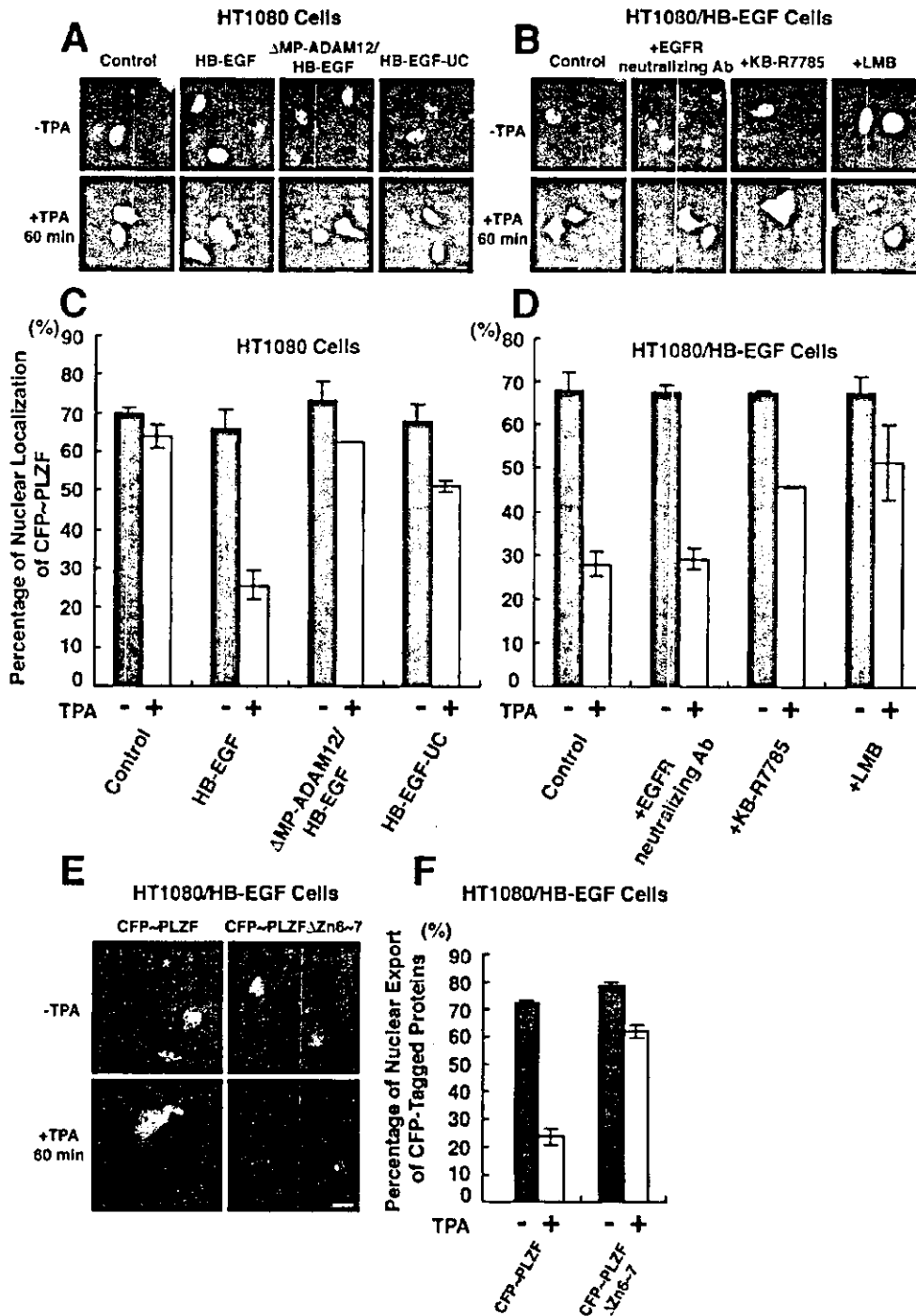
Figure 3. **Processing of proHB-EGF by ADAM12 causes nuclear export of PLZF.** Subcellular localization of CFP-PLZF fusion protein in HT1080 cells and its variants. The CFP-PLZF expression vector was transiently transfected into four types of cells: HT1080 cells (HT1080); proHB-EGF-overexpressing HT1080 cells (HT1080/HB-EGF); proHB-EGF- and metalloprotease domain-deleted mutant of ADAM12-overexpressing HT1080 cells (HT1080/ΔMP-ADAM12/HB-EGF); and uncleavable-type proHB-EGF-overexpressing HT1080 cells (HT1080/HB-EGF-UC). (A and C) 24 h after the transfection, CFP-PLZF was predominantly localized at the nucleus in these four cell types. In HT1080/HB-EGF cells (but not the other types of cells), CFP-PLZF was distributed in the entire cytoplasm after treatment of the cells with 100 nM TPA for 60 min (B and D). A metalloprotease inhibitor KB-R7785 (10 μM), but not an EGFR-neutralizing antibody (10 μg/ml), inhibited nuclear export of CFP-PLZF in HT1080/HB-EGF cells in response to treatment with TPA for 60 min. Note that nuclear export of CFP-PLZF was dependent on the processing of HB-EGF, but that EGFR signaling was not involved in this process. 10 ng/ml leptomycin B (LMB), a specific inhibitor of CRM1-dependent nuclear export, also inhibited nuclear export of CFP-PLZF after TPA treatment. (E and F) The expression vectors encoding CFP-PLZF (CFP-PLZF) or Zn6~7 deletion mutant of CFP-PLZF (CFP-PLZFΔZn6~7) were transiently transfected into HT1080/HB-EGF cells. After 24 h, changes in subcellular localization of CFP-tagged proteins after TPA treatment were examined. Note that the export of CFP-PLZFΔZn6~7 was suppressed in HT1080/HB-EGF cells after TPA stimulation. Bars, 10 μm.
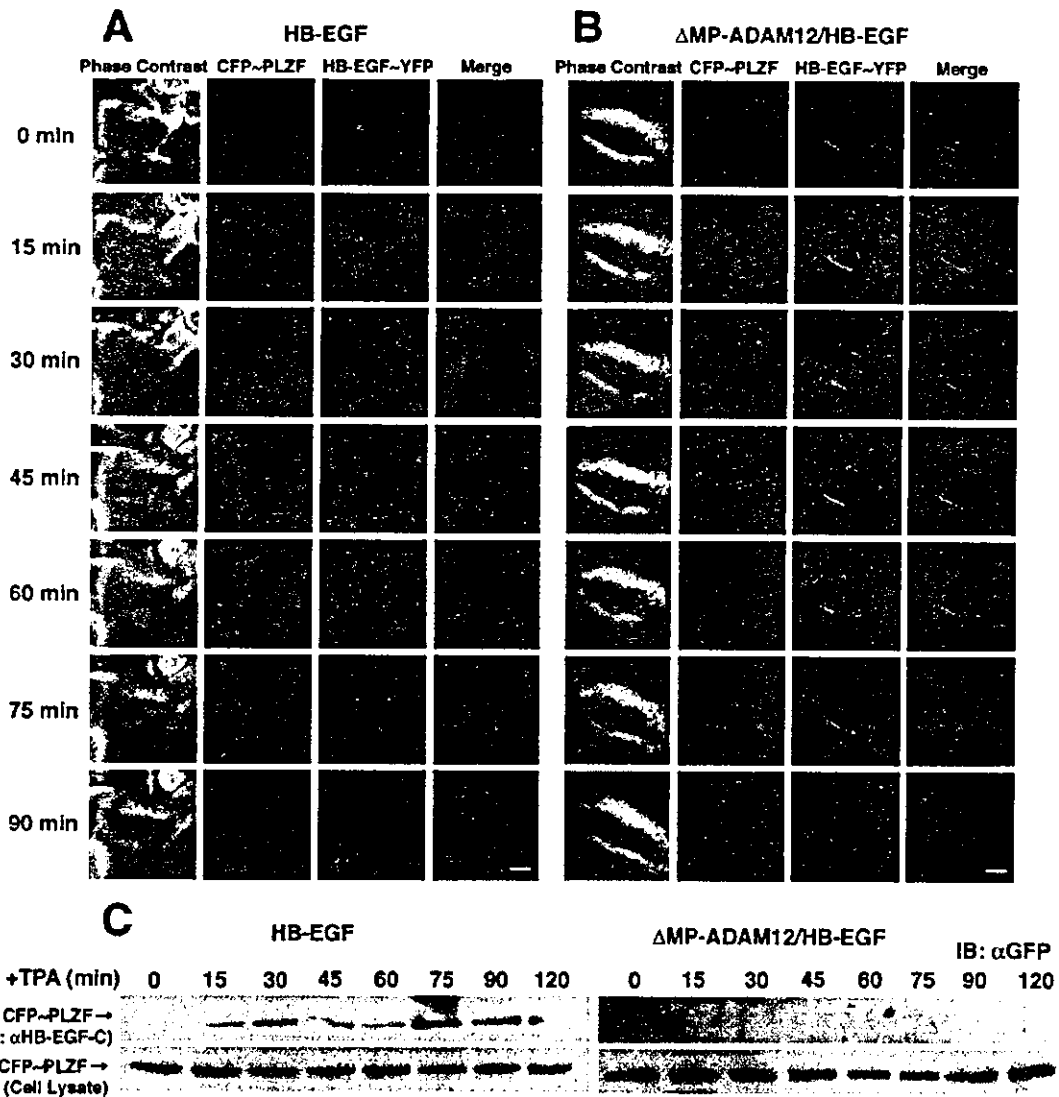
Figure 4. **Nuclear export of PLZF follows internalization of HB-EGF-C.** (A and B) Time-lapse imaging of CFP-PLZF and HB-EGF-YFP in living cells. Cells cotransfected with CFP-PLZF and HB-EGF-YFP expression vectors were cultured for 24 h before observation, and then the culture medium was replaced with medium containing 100 nM TPA. Shown are representative serial images of transfected HT1080/HB-EGF (A) and HT1080/ΔMP-ADAM12/HB-EGF (B) cells taken every 15 min up to 90 min after TPA stimulation. Note that translocation of HB-EGF-YFP preceded nuclear export of CFP-PLZF in HT1080/HB-EGF cells. Changes in subcellular localization of the CFP and YFP fusion proteins were not observed after TPA treatment of HT1080/ΔMP-ADAM12/HB-EGF cells. (C) Time course–dependent changes in interaction of HB-EGF-C with CFP-PLZF. The HB-EGF-C-PLZF interaction was investigated by immunoprecipitation using an anti-HB-EGF-C antibody in HT1080/HB-EGF and HT1080/ΔMP-ADAM12/HB-EGF cells. The band of CFP-PLZF coimmunoprecipitated with HB-EGF-C (top) was evident at 15 min and the later after TPA treatment in HT1080/HB-EGF but not HT1080/ΔMP-ADAM12/HB-EGF cells, despite same expression of CFP-PLZF in cells (bottom). Bars, 10 μm.

HB-EGF-YFP did not promote nuclear export of PLZF (unpublished data), possibly due to the fused YFP interfering with the interaction between HB-EGF-C and PLZF. Therefore, HB-EGF-YFP and CFP-PLZF expression vectors were cotransfected into HT1080/HB-EGF or HT1080/ ΔMP-ADAM12/HB-EGF cells that stably expressed wild-type proHB-EGF. Images were collected every 15 min up to 90 min after TPA treatment. In HT1080/HB-EGF cells, internalization of HB-EGF-YFP was observed 30 min after the treatment, but nuclear export of CFP-PLZF did not oc-

cur until 45 min after TPA stimulation (Fig. 4 A). In HT1080/ΔMP-ADAM12/HB-EGF cells, subcellular localization of HB-EGF-YFP and CFP-PLZF were not changed despite TPA treatment (Fig. 4 B).

Time course–dependent changes in interactions of HB-EGF-C with CFP-PLZF were investigated in these cells by immunoprecipitation experiments. Anti-HB-EGF-C antibody #H1 clearly coimmunoprecipitated CFP-PLZF at 15 min and the later with maximal binding at 30 and 75 min after TPA stimulation in HT1080/HB-EGF cells, but not in
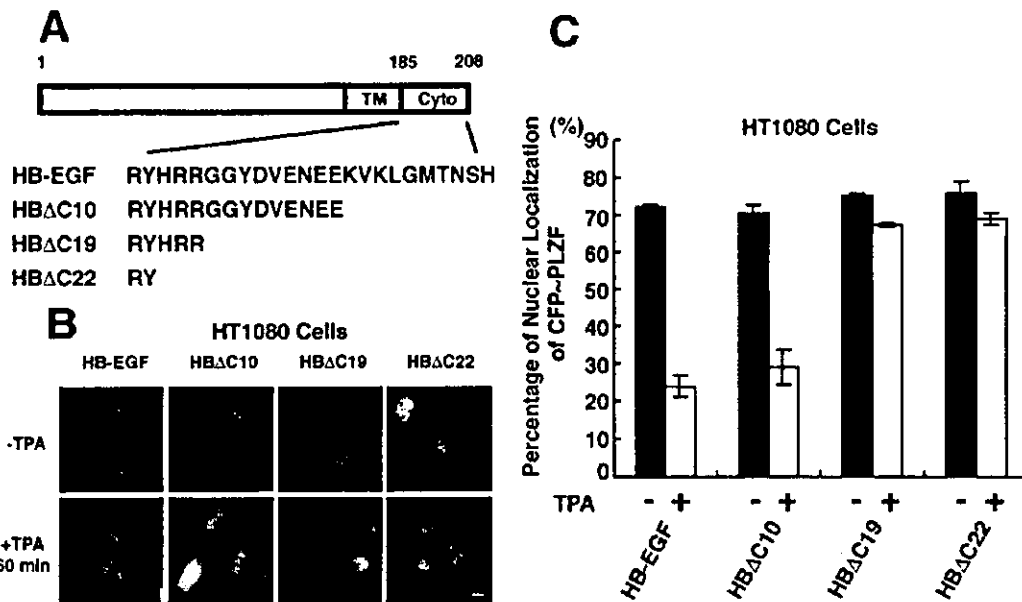
Figure 5. Cytoplasmic region of proHB-EGF is required for PLZF export after TPA stimulation. (A) Structures of cytoplasmic deletion mutants of proHB-EGF. These mutants, HBΔC10, HBΔC19, and HBΔC22, were truncated by 10, 19, and 22 amino acids, respectively, from the carboxy terminus of proHB-EGF. (B and C) Subcellular localization of CFP-PLZF in HT1080 cells stably expressing proHB-EGF and its cytoplasmic deletion mutants. CFP-PLZF was predominantly localized in the nucleus in these stable transfectants. In HT1080/HB-EGF and HT1080/HBΔC10 cells, TPA treatment distributed CFP-PLZF to the entire cytoplasm. However, in HT1080/HBΔC19 and HT1080/HBΔC22 cells, the export of CFP-PLZF from nucleus was not observed after TPA stimulation. Bar, 10 μm.

HT1080/ΔMP-ADAM12/HB-EGF cells (Fig. 4 C). These results, together with time-lapse images, indicate that internalized HB-EGF-C interacted with nuclear PLZF.

The proHB-EGF cytoplasmic region is required for PLZF transport

The data presented in Fig. 3 indicated that proteolytic release of HB-EGF-C by proHB-EGF processing could trigger the nuclear export of PLZF. Therefore, we designed three types of cytoplasmic deletion mutants of proHB-EGF (HBΔC10, HBΔC19, and HBΔC22; Fig. 5 A), constructed their expression vectors, and established stable transfectants of HT1080 cells with each of the vectors. All YFP-tagged deletion mutants of proHB-EGF were also localized at the plasma membrane and internalized into the cytoplasm by TPA treatment (unpublished data). HT1080/HBΔC10 cells (as well as HT1080/HB-EGF cells) showed TPA-responsible nuclear export of PLZF. However, in HT1080/HBΔC19 and HT1080/HBΔC22 cells, nuclear export of PLZF did not occur despite TPA stimulation (Fig. 5, B and C).

Increased expression of cyclin A and promotion of S-phase progression associated with nuclear export of PLZF

It has been reported that PLZF is a transcriptional repressor of cyclin A and inhibits cell growth (Shaknovich et al., 1998; Yeyati et al., 1999). HT1080/HB-EGF cells transfected with an expression vector for FLAG-tagged PLZF (FLAG-PLZF) were cultured for 48 h in the medium containing 3% serum, and then the culture medium was replaced with fresh medium with and without 100 nM TPA.

After 8 h, expression of both FLAG-PLZF and cyclin A was examined by immunofluorescence microscopy. The intensity of cyclin A immunofluorescence in the transfected cells expressing FLAG-PLZF (Fig. 6 A, arrows) was much less than that in untransfected cells (Fig. 6 A, arrowheads). TPA treatment distributed FLAG-PLZF into the entire cytoplasm and up-regulated the immunofluorescence intensity of cyclin A in the transfected cells (Fig. 6 A, arrows) to the same level as that in the untransfected cells (Fig. 6 A; arrowheads). The range of relative fluorescence intensity of cyclin A in TPA-treated cells was narrower than that in nontreated cells, and the reduced expression of cyclin A associated with nuclear-localized FLGA-PLZF was not observed (Fig. 6 B). However, in HT1080, HT1080/ΔMP-ADAM12/HB-EGF, and HT1080/HB-EGF-UC cells, FLAG-PLZF was localized in the nucleus and suppressed cyclin A expression in the absence or presence of TPA (unpublished data).

The effect of PLZF on cell cycle was investigated in HT1080 and HT1080/HB-EGF cells. To control cell cycle progression and proHB-EGF processing simultaneously, we synchronized the cells infected with the PLZF or LacZ expression adenoviruses in G0/G1-phase by serum deprivation, and then stimulated the cells back into cycle by addition of 10% serum. proHB-EGF processing is induced by serum-containing medium without any particular stimuli (Goishi et al., 1995; Hirata et al., 2001), and a large amount of released HB-EGF was detected in the conditioned medium of HT1080/HB-EGF cells (unpublished data). After the serum stimulation, the cells were collected every 4 h up to 24 h and analyzed for DNA content and cyclin A expres-
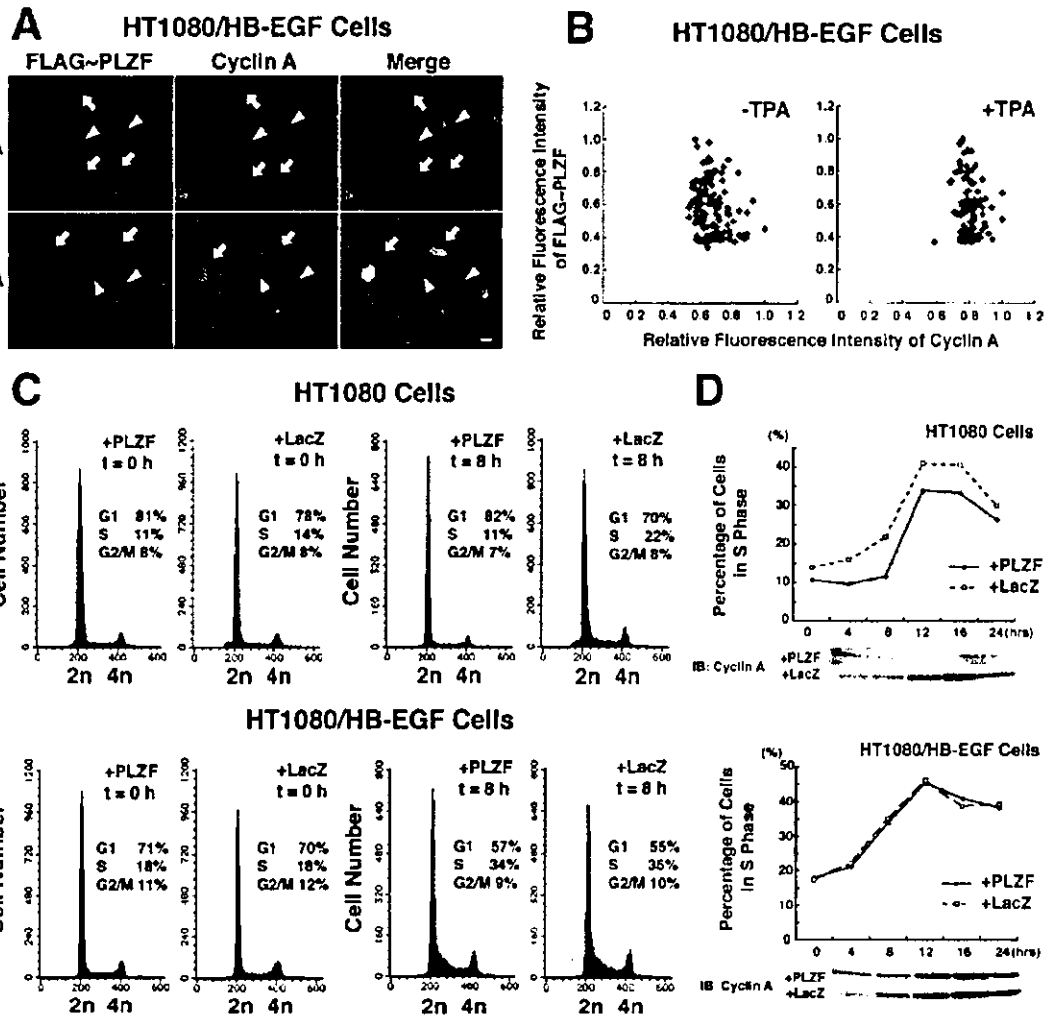
Figure 6. **Processing of proHB-EGF reverses PLZF-dependent cyclin A suppression and delayed entry of S-phase.** (A and B) Expression analysis of FLAG-PLZF and cyclin A by immunofluorescence microscopy. An expression vector encoding FLAG-tagged PLZF (FLAG-PLZF) was transiently transfected into HT1080/HB-EGF cells, and the expression of FLAG-PLZF and cyclin A was detected with anti-FLAG and anti-cyclin A antibodies, respectively. (A) In transfected cells (arrows), FLAG-PLZF was localized at the nucleus and suppressed cyclin A expression in the absence of TPA treatment. In the presence of TPA, FLAG-PLZF was distributed into the entire cytoplasm, and the expression level of cyclin A in the transfected cells (arrows) was the same as that in the untransfected cells (arrowheads). (B) Relative fluorescence intensity of cyclin A and FLAG-PLZF was measured at the nucleus of the transfected cells. (C and D) Cell cycle analysis by DNA staining and cyclin A immunoblotting. HT1080 cells and its variants infected with PLZF or LacZ (control) expression adenoviruses were synchronized in G0/G1-phase by serum deprivation for 36 h and were restimulated into cell cycle with 10% serum. At the indicated times, cells were collected and analyzed for cell cycle phase and cyclin A expression. (C) Exogenous expression of PLZF by adenovirus induced the delay of S-phase entry after the serum stimulation in HT1080, but not in HT1080/HB-EGF cells. Cells were stained with propidium iodide and analyzed by FACS® to determine their DNA content and cell cycle phase at 0 and 8 h after addition of 10% serum. Cell number is plotted on the y axes, and DNA content is plotted on the x axes. (D) The delay of S-phase entry and suppression of cyclin A expression were reversed by proHB-EGF processing. The percentage of cells in S-phase is plotted versus time after serum stimulation. Whole-cell lysates from HT1080 and HT1080/HB-EGF cells (10[5]) harvested at each point were immunoblotted with anti-cyclin A antibody. The expression of β-actin was examined as a control (not depicted). Bar, 10 μm.

sion by flow cytometry and immunoblotting, respectively. Entrance into S-phase was delayed in the PLZF-expressing HT1080 cells compared with the control LacZ-expressing HT1080 cells (Fig. 6, C and D). Consistent with the delay of S-phase entry, increased expression of cyclin A after the stimulation was suppressed in HT1080 cells expressing PLZF (Fig. 6 D). However, S-phase entry and cyclin A regulation were reversed in HT1080/HB-EGF cells expressing PLZF (Fig. 6, C and D).

Intracellular localization of HB-EGF-C in human keratinocyte cell line HaCaT and primary cultured cells

We examined human keratinocyte cell line HaCaT and primary cultured cells to determine the localization of endogenous HB-EGF-C. TPA treatment of HaCaT cells (Fig. 7 A) as well as primary cultured cells (unpublished data) resulted in the production of an ~6.7-kD band, the expected size of an HB-EGF-C retaining both the transmembrane and cyto-
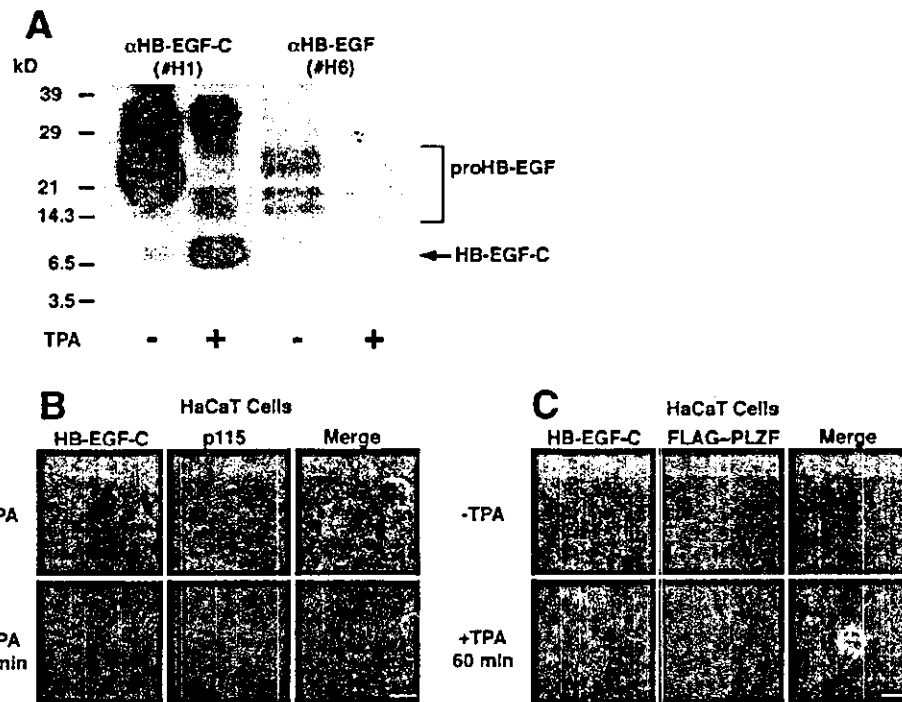
Figure 7. **Characterization of endogenous HB-EGF-C in HaCaT cells.** (A) Characterization of endogenous HB-EGF-C in untransfected HaCaT cells. 10^8 HaCaT cells that had been incubated in the presence or absence of TPA were lysed and immunoprecipitated with an HB-EGF-C antibody #H1, and the precipitates were immunoblotted with antibodies #H1 or #H6 (recognizing HB-EGF ectodomain). Both antibodies detected the 20–30-kD heterogenous bands of proHB-EGF. A 6.7-kD band was detected with the #H1 antibody, but not with #H6, and the density of this band was enhanced by TPA treatment. The apparent size of this band was consistent with the putative size of a form of HB-EGF-C containing the transmembrane and cytoplasmic domains of proHB-EGF. (B) Staining with the #H1 antibody showed that the cell surface HB-EGF–associated fluorescence was reduced once untransfected HaCaT cells were treated with TPA for 30 min. The perinuclear accumulation of HB-EGF-C, more evident after TPA treatment for 30 min, was colocalized with p115, a marker protein of the Golgi apparatus. (C) The plasmid encoding FLAG-PLZF was transiently transfected into HaCaT cells, and after 48 h, the localization of FLAG-PLZF and endogenous HB-EGF-C was visualized with immunofluorescent microscopy. HB-EGF-C accumulated and partially colocalized with FLAG-PLZF at the nucleus of HaCaT cells after 30 min of TPA treatment. Bars, 10 μm.

plasmic domains of proHB-EGF. HB-EGF-C was in the Golgi apparatus after 30 min of TPA treatment, as determined by its colocalization with the Golgi protein p115 (Nelson et al., 1998; Fig. 7 B). HB-EGF-C accumulated and partially colocalized with FLAG-tagged PLZF at the nucleus of HaCaT cells after 60 min of TPA treatment (Fig. 7 C).

Gene expression of PLZF was detected by RT-PCR in human primary keratinocytes, but not in HT1080 or HaCaT cells (unpublished data). Immunostaining of endogenous HB-EGF-C, PLZF, and cyclin A in primary cultured keratinocytes revealed their complemental localization in nucleus, cytoplasm, and plasma membrane under different conditions (Fig. 8 A). Keratinocytes in culture medium supplemented with bovine brain extracts showed heterogeneous staining of HB-EGF-C, PLZF, and cyclin A. However, TPA treatment clearly localized HB-EGF-C in nuclei and PLZF in the cytoplasm (Fig. 8, A and B). On the other hand, KB-R7785 treatment mainly localized HB-EGF at the plasma membrane and PLZF in the nuclei despite the addition of TPA (Fig. 8 A). Cyclin A was detected in the nuclei of most cells in response to the nuclear export of PLZF (Fig. 8 A). Increased expression of cyclin A in cultured keratinocytes after proHB-EGF processing was also confirmed by immuno-

blotting (Fig. 8 C). Further, treatment with angiotensin II, which causes GPCR-mediated EGFR transactivation through proHB-EGF processing in keratinocytes (unpublished data), also triggered the localization of HB-EGF-C in nuclei and PLZF in the cytoplasm, which was canceled effectively by the addition of KB-R7785 (Fig. 8 D).

Immunoprecipitation of PLZF in primary cultured keratinocytes resulted in the coprecipitation of HB-EGF-C, and the amount of the coprecipitated HB-EGF-C increased when the cells were incubated with TPA before lysis (Fig. 8 E). Thus, the interaction between PLZF and HB-EGF-C also occurs in primary cells. Similarly, anti-HB-EGF-C antibody #H1 also coimmunoprecipitated PLZF in the same cells (Fig. 8 E).

PLZF-HB-EGF-C interaction in vivo

We also examined the interaction of PLZF and HB-EGF-C in vivo using a TPA-treated mouse skin model of keratinocyte hyperplasia. TPA treatment of mouse skin tissue for 24 and 48 h produced keratinocyte hyperplasia as reported previously (Hawighorst et al., 2001; Fig. 9 A). Immunoprecipitation of PLZF in the homogenates of TPA-treated and control mouse skin tissues resulted in the coprecipitation of a 6.7-kD band recognized by anti-HB-EGF-C anti-
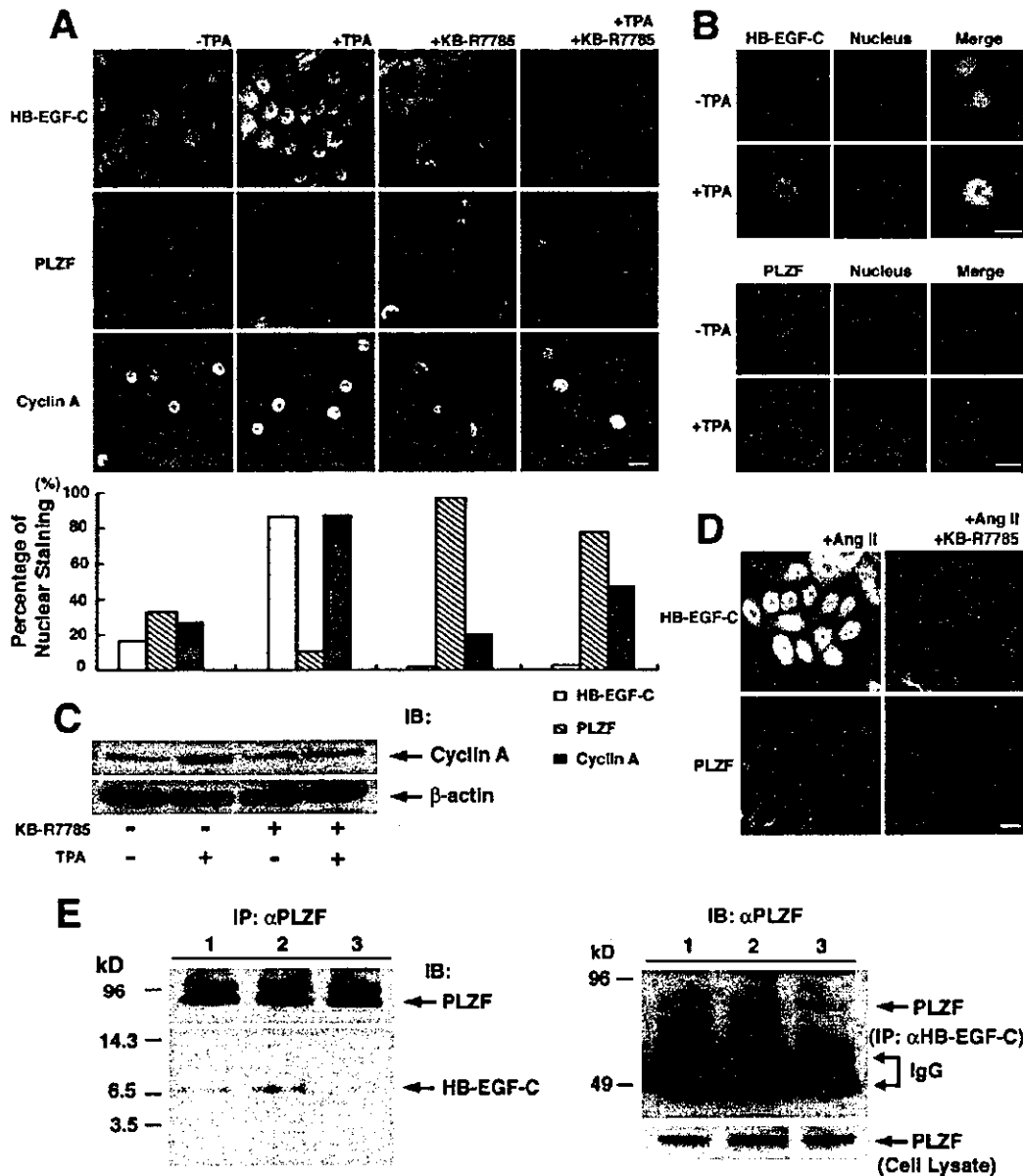
Figure 8. Interaction and traffic of endogenous HB-EGF-C and PLZF in human primary cultured keratinocytes. (A) Detection and localization of endogenous HB-EGF-C, PLZF, and cyclin A in primary human cultured keratinocytes by immunofluorescence microscopy. Keratinocytes were cultured in medium supplemented with bovine brain extracts and stained with antibodies against HB-EGF-C, PLZF, and cyclin A. Heterogeneous staining of HB-EGF-C, PLZF, and cyclin A was observed under the normal culture conditions. However, TPA treatment clearly localized HB-EGF-C in nuclei and PLZF in the cytoplasm, and up-regulated the expression of cyclin A in nuclei. KB-R7785 treatment resulted in HB-EGF-C staining at the plasma membrane and PLZF staining in nuclei despite the addition of TPA. (B) Nuclear accumulation of HB-EGF-C and export of PLZF after TPA stimulation. To facilitate the changes in subcellular localization of HB-EGF-C and PLZF after TPA treatment, we performed a nuclear staining using Hoechst 33258 in combination with immunostaining using anti-HB-EGF-C or PLZF. (C) Analysis of cyclin A expression in primary human cultured keratinocytes by immunoblotting. Consistent with immunostaining data, increased expression of cyclin A was observed in the keratinocytes treated with TPA. KB-R7785 suppressed cyclin A expression despite TPA stimulation. The expression of β-actin was examined as a control. (D) Staining of HB-EGF-C in nuclei and PLZF in the cytoplasm was also observed after angiotensin II treatment of the cells for 6 h, and this effect was reversed by the addition of KB-R7785 to the medium. (E) Interaction of HB-EGF-C and PLZF in human primary cultured keratinocytes. Cell lysates (10^7 cells) were immunoprecipitated with anti-PLZF antibody and immunoblotted with anti-PLZF (top left) and HB-EGF-C #H1 (bottom left) antibodies. Coimmunoprecipitated HB-EGF-C was slightly detectable in lysates from cells in normal culture conditions (lane 1), but the intensity of this band was increased by TPA treatment (lane 2). Addition of KB-R7785 (lane 3) resulted in the loss of the HB-EGF-C from the PLZF immunoprecipitates. Anti-HB-EGF-C antibody #H1 also coimmunoprecipitated PLZF (top right; each lane indicates the same condition as in left panel). PLZF was equally present in each cell lysate, as shown by Western blotting (bottom right). Bars, 10 μm.
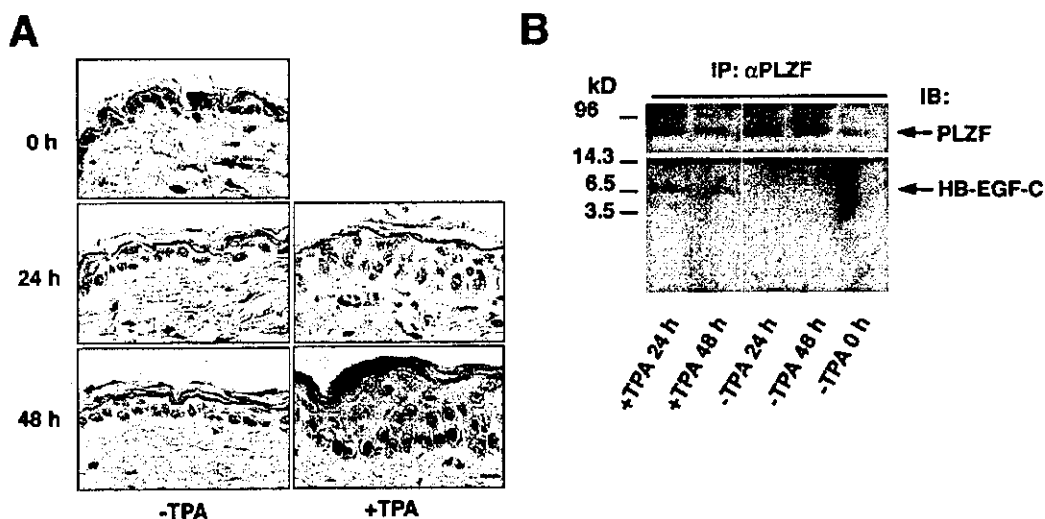
A

B

Figure 9. Involvement of the HB-EGF-C–PLZF interaction in epidermal hyperplasia. In vivo interaction between HB-EGF-C and PLZF in TPA-treated mouse skin hyperplasia. (A) Mouse skin was treated with TPA, and keratinocyte hyperplasia was successively observed for 48 h by HE staining. (B) The homogenates of TPA-treated and control mouse skin tissues were immunoprecipitated with anti-PLZF antibody and immunoblotted with anti-PLZF (top) or HB-EGF-C #H1 (bottom) antibodies. A 6.7-kD band identified as HB-EGF-C was detected in TPA-treated tissue homogenates, but not in control skin tissues. Bar, 10 μm.

body #H1 in TPA-treated tissue homogenates alone (Fig. 9 B), suggesting that the PLZF-HB-EGF-C interaction occurs in vivo.

Discussion

The biological functions of the EGFR ligand HB-EGF, shed by proteolytic cleavage from the amino terminus of the transmembrane proHB-EGF, have been well studied. In contrast, roles of the carboxy-terminal fragment (HB-EGF-C) produced by proHB-EGF processing have not been previously investigated. Our present work has three major findings concerning HB-EGF-C. First, HB-EGF-C generated by ectodomain shedding of proHB-EGF is translocated from the plasma membrane to the nucleus. Second, the proteolytic release of HB-EGF-C results in nuclear export of the transcriptional repressor PLZF. Third, cell cycle regulation by nuclear PLZF is reversed by proHB-EGF processing.
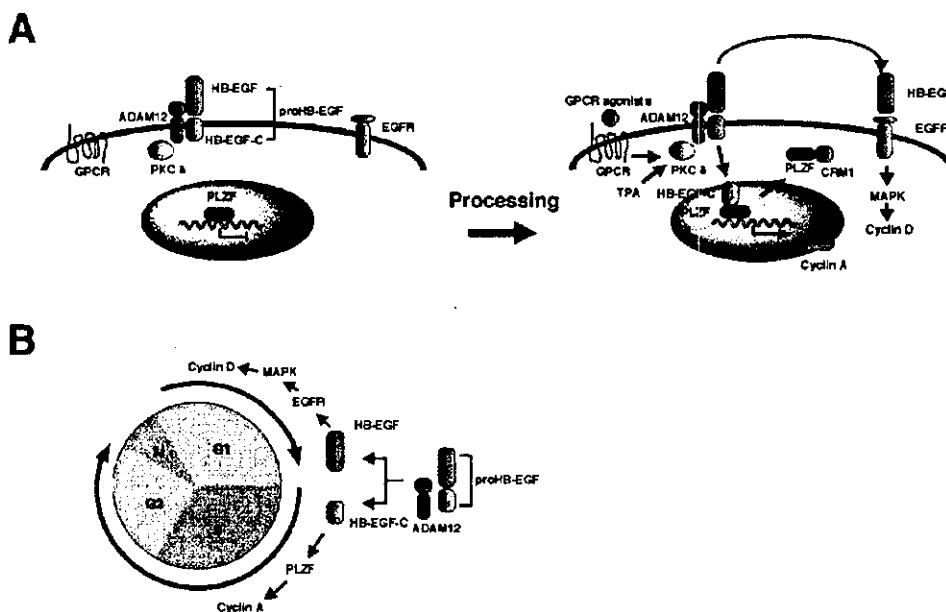
A

B

Figure 10. Schematic models of the roles of HB-EGF-C. (A) An intracellular signaling mediated by HB-EGF-C produced by proHB-EGF processing. (B) Coordination of cell cycle progression by shed HB-EGF and HB-EGF-C.

Using the technology of fluorescent proteins, we first demonstrated that HB-EGF-C was internalized into the cytoplasm after ectodomain shedding. Immunoblotting of the nuclear fraction and immunostaining using the antibody recognizing the cytoplasmic region of proHB-EGF (#H1) revealed the accumulation of endogenous HB-EGF-C in the nucleus after the processing. The 6.7-kD band of HB-EGF-C and no effect of dominant-negative presenilin-1 on HB-EGF-C translocation indicate that HB-EGF-C has the proHB-EGF transmembrane domain and is not further processed by γ-secretase. The colocalization of HB-EGF-C with p115, a marker protein of the Golgi apparatus, indicates that it is internalized by vesicular trafficking. Although the detailed transport mechanism of HB-EGF-C containing transmembrane domain remains unclear, recent analyses of nuclear localization of receptor tyrosine kinases raise the possibility that the Golgi–ER pathway is a route to the nucleus of type I transmembrane molecules (Carpenter, 2003). As shown in Fig. 1, TPA treatment localized HB-EGF–YFP around the nucleus, but not in the nucleus. HB-EGF–YFP did not promote the nuclear export of PLZF after TPA treatment (unpublished data). Therefore, we speculate that the YFP moiety fused to the carboxy terminus of HB-EGF-C might aggregate and fail to enter the nucleus, which abrogates the HB-EGF-C–PLZF interaction.

Recently, it has been reported that neuregulin-1 is cleaved at the transmembrane domain and the released intracellular domain (Nrg-1-ICD) enters the nucleus to repress expression of several regulators of apoptosis (Bao et al., 2003). Bao et al. (2003) also mentioned that Nrg-1-ICD forms the complex with a second zinc finger–containing protein related to PLZF. Although the machinery of carboxy-terminal signaling of proHB-EGF and neuregulin-1 seems to be different, these results, together with our present data, suggest that the carboxy-terminal fragments of the EGF family precursors are functional molecules that control gene expression by regulating transcription factors in the nucleus.

It is apparent that nuclear accumulation of HB-EGF-C, nuclear export of PLZF, and interaction between HB-EGF-C and PLZF are mutually exclusive. Although the machinery of this signaling is still unclear, one possible mechanism suggested by time course–dependent changes in the interaction and localization of HB-EGF-C and PLZF is as follows: (1) HB-EGF-C is translocated into the nucleus after proHB-EGF processing; (2) HB-EGF-C associates with nuclear PLZF; and (3) PLZF is exported from the nucleus in a CRM1-dependent manner (Fig. 10 A).

The cleavage of proHB-EGF is required for EGFR transactivation in response to GPCR signaling (Prenzel et al., 1999, Asakura et al., 2002, Chen et al., 2002; Cussac et al., 2002; Lemjabbar and Basbaum, 2002), suggesting that posttranslational processing of proHB-EGF is involved in a variety of biological processes. In the present report, we show that nuclear export of PLZF also results from angiotensin II stimulation in human primary cultured keratinocytes. This result suggests that proHB-EGF processing by the GPCR signaling cascade leads to the nuclear export of PLZF. PLZF is expressed in a large number of tissues, and perinatal upregulation of this factor is observed in the kidney, liver, and heart (Cook et al., 1995; Reid et al., 1995). PLZF produces

transcriptional repression through recruitment of a repressor complex that contains N-CoR, SMRT, Sin3a, and histone deacetylase (Hong et al., 1997; David et al., 1998; Grignani et al., 1998; Guidez et al., 1998; He et al., 1998; Lin et al., 1998). The study of PLZF knockout mice indicates that PLZF represses Hox gene expression though chromatin remodeling to regulate the patterning of limb and axial skeleton, and is involved in apoptosis and cell proliferation during limb development (Barna et al., 2000, 2002). Thus, these findings suggest potential roles for HB-EGF-C mediated nuclear export of PLZF and the subsequent effects on regulation of cell proliferation and Hox gene expression in various signaling cascades during the development and maintenance of adult tissues.

It has been reported that PLZF is a transcriptional repressor of cyclin A and suppresses cell growth by inhibiting entry or progression of S-phase in the cell cycle (Shaknovich et al., 1998; Yeyati et al., 1999). Gene expression control by transcriptional regulators occurs in the nucleus, and nuclear export of these factors results in loss of the regulation. The present data show that HB-EGF-C generated by ectodomain shedding of proHB-EGF causes nuclear export of PLZF, increases the expression of cyclin A, and promotes S-phase entry. Furthermore, the interaction of HB-EGF-C and PLZF occurs in the TPA-treated mouse skin model of keratinocyte hyperplasia. On the other hand, proHB-EGF processing also generates HB-EGF, a soluble ligand of EGFR. It is well known that HB-EGF activates EGFR signaling and promotes G1-phase progression in the cell cycle by regulating the expression of cyclin D via the Ras-MAPK signaling cascade (Hackel et al., 1999; Prober and Edgar, 2001). Therefore, our current paper suggests that proHB-EGF has two functional domains affecting mitogenic signaling. Posttranslational processing of proHB-EGF by metalloprotease activation produces intercellular and intracellular signaling molecules simultaneously (Fig. 10 A). The coordination of the resulting dual mitogenic signals may be important for cell cycle progression in various signaling cascades (Fig. 10 B).

Materials and methods

Plasmid construction
A plasmid for recombinant expression of YFP-tagged proHB-EGF was generated by subcloning the human HB-EGF cDNA with the stop codon deleted into pEYFP-N1 (CLONTECH Laboratories, Inc.). A plasmid for recombinant expression of CFP-tagged PLZF was generated by subcloning the human PLZF cDNA into pECFP-C1 (CLONTECH Laboratories, Inc.). DNA fragments encoding the deleted cytoplasmic region of proHB-EGF with or without stop codon were generated by PCR and substituted for the corresponding region in pEYFP-N1-HB-EGF. A plasmid encoding FLAG-tagged PLZF was generated by subcloning the FLAG sequence and the human PLZF cDNA into pcDNA3.1 (Invitrogen). pcDNA3.1/FLAG/PS1(D385A) was a gift from Dr. Okochi (Osaka University, Osaka, Japan). Plasmids for recombinant expression of FLAG-tagged PLZF derivatives were generated by subcloning the FLAG and various PLZF derivative sequences made by PCR into pME18S. A plasmid for recombinant expression of GST-fused HB-EGF-C was generated by subcloning the HB-EGF-C sequence made by PCR into pGEX6P-1 (Amersham Biosciences). All cDNA constructs were verified by DNA sequencing.

Yeast two-hybrid assay
The cytoplasmic domain of proHB-EGF (residues 185–208; Higashiyama et al., 1991) was used to screen a human heart cDNA library in the yeast two-